Modification and validation of a commercial dynamic chamber for reactive nitrogen and greenhouse gas flux measurements

Moxy Shah[1], Kifle Z. Aregahegn[1], Danial Nodeh-Farahani[1], Leigh R. Crilley[1,‡], Tasnia Hasan[1], Yashar Ebrahimi-Iranpour[1], Fahim Sarker[1], Nick Nickerson[2], Chance Creelman[2], Sarah Ellis[2], Alexander Moravek[1,§], Trevor C. VandenBoer[1,*]

[1] Department of Chemistry, York University, Toronto, Ontario, Canada

[2] Eosense Inc., Dartmouth, Nova Scotia, Canada

[‡] Now at: Atmospheric Services, WSP Australia, Brisbane, QLD, Australia

[§] Now at: German Environment Agency, Department of Air Quality, Dessau-Rosslau, Germany

[*]Communicating author: tvandenb@yorku.ca

Abstract

Reactive nitrogen gases (NO, NO_2, HONO, NH_3 and others; N_r) play important roles in atmospheric processes, and their cascading impacts throughout the Earth system have adverse effects on both the environment and human health. The fluxes of these gases at the surface-atmosphere interface have been studied in isolation or smaller subsets, but simultaneous fluxes of all N_r alongside standard greenhouse gases (GHGs) have not been reported. Here, a dual-dynamic chamber system was developed for N_r by modifying a commercially available system for GHG fluxes for use with destructive analyzers. It includes a reference chamber to account for chemical reactions and surface interactions. The resulting platform makes the measurement of N_r and by extension, other reactive gases, more widely accessible to the scientific community because custom chambers do not need to be fabricated.

System modifications to passivate surfaces reduced an initial 36% loss of NO_2 to below analyzer detection limits (~10%) for relevant atmospheric conditions. The modified 72 L chamber response times (τ) did not change for GHGs or NO (τ = 37-39 min versus a theoretical 36 min) at a flow rate of 2 L min^{-1}. The modifications improved the transfer of NO_2, HONO, and NH_3 by up to 2

min, but substantial surface interactions for NH_3 remain. A surface interaction term was characterized for these gases to obtain accurate field fluxes via a mass balance framework.

Proof-of-concept measurements of N_r fluxes from agricultural soil samples under controlled lab conditions as a function of soil water content were able to quantify emissions of NO, NO_2, HONO, NH_3, and N_2O simultaneously. We observed soil fluxes without amendment and when subject to N_r fertilization. Unfertilized soils showed variability in NO_2 and HONO emissions when soil structure was minimally disturbed, consistent with in-situ field measurements from other researchers. These oppose maximum potential fluxes in prior lab soil manipulations, particularly for HONO relative to NO. Last, N_r field fluxes were quantified with the dual-chamber system on an in-use agricultural soil, including baseline conditions and a urea-based fertilizer perturbation to stimulate microbial and chemical transformation and transfer N_r to the atmosphere. Good agreement with other field flux techniques was found. The mass balance terms within the dual-chamber approach are fully inspected from the pilot deployment in the field, along with an error analysis, to aid in the uptake of this approach by the community.

1 Introduction

Earth's biogeochemical nitrogen (N) cycle is essential for sustaining life through the production of nucleic acids, proteins, and other vital biomolecules (Lehnert et al., 2021). The carbon cycle receives much focus due to the climate impacts of greenhouse gases (GHGs) like carbon dioxide (CO_2) and methane (CH_4), yet the N cycle is intertwined (Schlesinger, 2020). At the interface of these cycles and the Earth's surface, reactive nitrogen (N_r) species exchanged between ecosystems and the atmosphere have therefore become an area of emerging interest (Lehnert et al., 2021; Wu et al., 2020). Atmospheric N_r species such as nitric oxide (NO) and nitrogen dioxide (NO_2) – collectively referred to as NO_x – ammonia (NH_3), and nitrous acid (HONO) can experience surface-atmosphere exchange, impacting local air or water quality, ecosystem processes, and biodiversity (Lehnert et al., 2021; Richardson et al., 2023; Wu et al., 2020). Meanwhile, the non-reactive nitrous oxide (N_2O) has climate impacts due to its ~120-year lifetime (IPCC, 2023).

Reactive nitrogen gases play important roles in atmospheric processes, contributing to the formation of pollutants like ozone (O_3) and secondary organic aerosols (SOA). The exchange of N_r between the Earth's surface and the atmosphere involves production and loss processes driven by both natural and human activities. They are removed through wet and dry deposition, and their abundance reflects the net outcome relative to emissions (Delaria & Cohen, 2023). At the surface, N_r is released into the atmosphere by microbial nitrogen cycling, agricultural activities, wildfires, or fossil fuel combustion (Benedict et al., 2017; Mosier, 2008; Yang et al., 2024). Studying N_r at the surface-atmosphere interface with high time resolution and chemical speciation remains a challenge due to its high spatial and temporal variability driven by factors like climate, vegetation cover, and soil/surface properties (Ludwig et al., 2001). For example, vertically resolved HONO production at the ground surface demonstrated how it plays a major role in the unexplained daytime HONO source and its impact on daytime hydroxyl radical (OH) levels (VandenBoer et al., 2013, 2015; Young et al., 2012). Such observations pose a challenge because suitable high time resolution equipment is expensive, preventing the interplay between emission and deposition for all N_r species from being studied concurrently. As a result, no systems are sufficiently accessible to the scientific community to be deployed widely across different global landscapes, particularly soils.

Soils function as both a source and a sink of N_r. Soil-atmosphere exchange of N_r is governed by atmospheric abundance and/or soil microbial processes such as nitrification and denitrification, with factors like pH, moisture, organic matter, and nitrogen availability regulating flux directionality (Mosier, 2008; Purchase et al., 2023; Stepniewski et al., 2015). Microbial processes can drive the formation and release of N_r species like NO, NH_3 and N_2O from soils, and similar assertions with respect to HONO have been made (Butterbach-Bahl & Dannenmann, 2011; Kool et al., 2010; Mushinski et al., 2019; Oswald et al., 2013; Su et al., 2011). Understanding the exchange of all N_r gases is essential for unravelling the complex interactions between the nitrogen and carbon cycles and their broader environmental impacts (Richardson et al., 2023, Fowler et al., 2013).

Various flux measurement techniques have been employed to quantify N_r exchange for subsets of species. Quantifying fluxes has been most effectively applied to GHGs at the surface-atmosphere interface. Traditional measurement methods, such as eddy covariance (EC), relaxed eddy

accumulation (REA), and aerodynamic gradient (AG) methods, have been extensively used for ecosystem-scale, continuous flux monitoring, including targeted assessment of most N_r species (e.g., Bao et al., 2022; Geddes & Murphy, 2014; Kamp et al., 2020; Laufs et al., 2017; Min et al., 2014; Moravek et al., 2014, 2019; Ren et al., 2011; Von Der Heyden et al., 2022; Wang et al., 2022; Wolff et al., 2010). These micrometeorological techniques measure concentrations, concentration gradients, and/or turbulence to estimate fluxes across interfaces applicable to ecosystem-scale processes. When operated continuously, they offer long-term insight without disrupting the natural system. Chamber methods have some advantages compared to micrometeorological techniques, as they are relatively inexpensive, easy to deploy, and require minimal prior meteorological training and expertise (Tang et al., 2020). Chambers are limited to small plots, making them suitable to study the effect of different fertilizer treatments on agricultural soils, for example (Anthony & Silver, 2024; Chiaravalloti et al., 2023; Manco et al., 2025; Tang et al., 2020). The chamber method is widely used for GHG fluxes, especially N_2O. However, challenges remain in addressing potential biases introduced by chemical transformations within a chamber and interactions with the surfaces, particularly for N_r species such as NO_2, HONO, and NH_3.

Chemical transformations can occur on all surfaces between the point of emission and measurement, where surface interactions such as adsorption, desorption, and heterogeneous reactions can alter the apparent concentration. For example, NO could react with O_3 to form NO_2 during the day and NO_3 at night if sufficient O_3 is present to fully titrate NO (R1, R2). Heterogeneous reaction of gas-phase NO_2 on surfaces under humid conditions also produces nitric acid (HNO_3) and HONO (R3), although the real-world mechanism is not second order and remains uncertain (Kleffmann et al., 2005; Ramazan et al., 2004; VandenBoer et al., 2015). The formed HONO can undergo multiphase processes by partitioning into water according to its Henry's Law constant and then dissociating into nitrite (NO_2^-) and the hydronium ion (H_3O^+) according to its acid dissociation equilibrium constant and the pH (R4, R5) (He et al., 2006; Ren et al., 2020). Nitrous acid could also photolyze, yielding NO and OH (R6) (Spataro & Ianniello, 2014).

$$NO + O_3 \rightarrow NO_2 + O_2 \quad \text{(R1)}$$

$$NO_2 + O_3 \rightarrow NO_3 + O_2 \quad \text{(R2)}$$

$$2NO_{2\,(g)} + H_2O_{\,(ads)} \rightarrow HONO_{\,(g)} + HNO_{3\,(ads)} \quad \text{(R3)}$$

$$HONO_{\,(g)} \leftrightarrow HONO_{\,(aq)} \quad \text{(R4)}$$

$$HONO_{\,(aq)} + H_2O_{\,(l)} \rightleftharpoons NO_2^-{}_{(aq)} + H_3O^+{}_{(aq)} \quad \text{(R5)}$$

$$HONO + h\nu \rightarrow NO + OH \quad \text{(R6)}$$

These processes in/on the chamber and downstream surfaces can introduce uncertainty in flux measurements. Characterizing and accounting for chemistry and surface effects in chamber-based flux methods are therefore necessary. Static chamber systems typically determine the flux from the change in headspace concentration after closing the lid. Dynamic chamber systems have traditionally used a controlled flow of ambient air through the headspace to retrieve the flux from a concentration difference between the chamber inlet and outlet. The dynamic chamber flux method has measured challenging gases like biogenic volatile organic compounds, such as monoterpenes and isoprene, from vegetation and farmland (Kolari et al., 2012; Mochizuki et al., 2018, Pugliese et al. 2023), NH_3 volatilization from cattle manure (Becciolini et al., 2024), N_2O and NO_x from turfgrass (Maggiotto et al., 2000), and NO_x from grasslands (Pape et al., 2009; Plake et al., 2015). Scharko et al. (2015) used sealed chambers, while Tang et al. (2019) used dynamic, to highlight the hotspot potential for both HONO and NO_x fluxes from agricultural soils. These are of high interest due to their impacts on atmospheric chemistry from local to regional scales.

For example, the complex biological and chemical controls on nitrite (NO_2^-) production and loss in soils, coupled with soil properties facilitating gas exchange of HONO, has led to intense interest and debate around discerning the fundamental controls on its surface-atmosphere exchange (R4, R5) (Barney & Finlayson-Pitts, 2000; Huang et al., 2002; Kamboures et al., 2008; Meusel et al., 2018; Mushinski et al., 2019; Purchase et al., 2023; Song et al., 2023; Sörgel et al., 2015; Wang et al., 2021). The same is true for direct emissions of NO_2 from soils, where evidence remains limited, and the uncertainty is high (Huber et al., 2024; Zörner et al., 2016). For example, Gong et al. (2025) estimate that fertilizer-induced soil NO_x emissions contribute 0.84–2.20 Tg N yr^{-1} globally. The large uncertainty is partly due to a lack of NO_2 measurements. Their modelling suggests this underestimates summertime ozone enhancements by 0.3–3.3 ppbv in agricultural hotspot regions, and has been implemented in atmospheric models (Ha et al., 2023; Tian et al.,

2024). Thus, N_r exchange in agricultural regions subject to elevated levels through excessive nitrogen inputs is a prime target for chamber methodologies (Degaspari et al., 2020; Huber et al., 2020; Manco et al., 2025). These knowledge gaps highlight the need for more field-based soil NO_2 and HONO flux measurements, alongside simultaneous constraints on the entire N_r suite.

Automated dynamic chambers deployed in situ for field observations and to conduct controlled experiments could capture the magnitude, direction, and temporal variability of N_r species and physical variables while retaining soils in an intact state (Aneja et al., 2006). Thus, establishing an accessible dynamic chamber method for N_r flux measurements is desirable. However, such a platform needs to undergo extensive validation to reduce flux bias from challenging N_r species such as NH_3. This important and necessary first step will allow a wider global study of surface-atmosphere N_r exchange processes. One of the best existing examples to date of automated dynamic chamber design for N_r measurements, is the custom-built system from Pape et al. (2009) who measured NO, NO_2, and O_3 to deploy an unattended array of six samplers with destructive gas analyzers. In their system, a reference chamber was used to characterize system surface effects, while using a large volume flow through the headspace during chamber closure periods to quantify fluxes on the assumption that ambient levels were not dramatically changing (e.g. due to nearby point sources). This work synthesized many advantages from similar designs to study soil- and plant-atmosphere interactions, but the technique remains accessible only to researchers with in-house engineering design and fabrication facilities. In the intervening years, dynamic chambers for GHG fluxes have become widely commercialized to improve measurement capacity compared to static chamber determinations and to make flux observations more accessible compared to conducting EC measurements.

Here, we bridge several gaps to link the atmospheric GHG and N_r flux communities with a dynamic flux system for CO_2, CH_4, N_2O, NO, NO_2, HONO, and NH_3. First, we modify commercial dynamic chambers with large volume (72 L) and footprint (0.21 m^2) originally designed for trace GHG flux measurements to make them suitable for quantifying the most prevalent N_r gas exchange fluxes at surface-atmosphere interfaces, meaning the apparatus is more widely available to the atmospheric community. Next, we implement surface and hardware modifications to adapt the commercial chambers to minimize gas adsorption and transformations, so that more reactive gases such as HONO and NH_3 can be added to the N_r flux analyte suite. We systematically characterized

the transfer of both GHGs and N_r species by calculating fill and empty rates, transformed to time constants, to identify and minimize surface interactions and/or transformations on the chamber surfaces. We then applied our modified commercial dynamic chambers to make flux measurements by equipping them with destructive gas analyzers for HONO and NO_x and a Picarro G2509 cavity ring-down spectrometer for NH_3, N_2O, CO_2, and CH_4 in lab experiments, or under field conditions with a fully automated dual-chamber approach in a pilot study with 30 minute closures to obtain a sufficient number of measurements to detect relevant fluxes with standard gas analyzers. Fluxes during the pilot study were assessed by rate of change determinations during closure periods and bias minimized through a mass balance to demonstrate system capabilities for several N_r gases in an agricultural field. This community-accessible approach addresses key needs by allowing more researchers to measure N_r exchange at the surface-atmosphere interface, with the added benefit over past systems to monitor fluxes of all species simultaneously with at least hourly time resolution when using gas analyzers with one-minute measurement frequencies.

2. Materials and methods

2.1 Dynamic Chambers for Field Fluxes

2.1.1 Description of custom-modified dual-dynamic chambers fluxes

The dynamic chamber system uses two identical commercially available units (eosAC-LT Eosense, Dartmouth, NS). These are modified and coupled to programmable valves that control sample gases delivered to a suite of instrumentation (Figure 1**)**.

The dynamic chambers are constructed with transparent polyacrylate walls and lids, with an internal volume of 0.072 m^3 (72 L) and bottom surface area of 0.21 m^2. When used on soils the chambers are secured with collars and custom-made polytetrafluorethylene (PTFE) rings (Figure S1). A built-in fan ensures uniform distribution of gases inside the chamber. Air temperature is measured inside from the fan arm, pressure is from the control box outside the chamber, and two auxiliary ports, one internal and external, can collect environmental properties such as relative humidity (RH), photosynthetically active radiation (PAR), soil temperature, and/or soil volumetric water content (VWC).

For an N_r sampling approach, one chamber is used as the measurement (MC) from an experimental surface while the second is a reference (RC) sealed at the bottom with a 51 µm (0.002”) film of perfluoroalkoxy alkane (PFA; McMasterr-Carr®, PN: 84955K24). The inert PFA film is held in place between the chamber collar and our custom-made PTFE rings (Figure S1). The RC acts as a negative control for physical interactions and/or associated chemistry of reactive gases on chamber and gas transfer line surfaces. The use of the RC, therefore, is to facilitate the correction of surface-mediated effects, reactions, and reduction of bias when determining flux values.

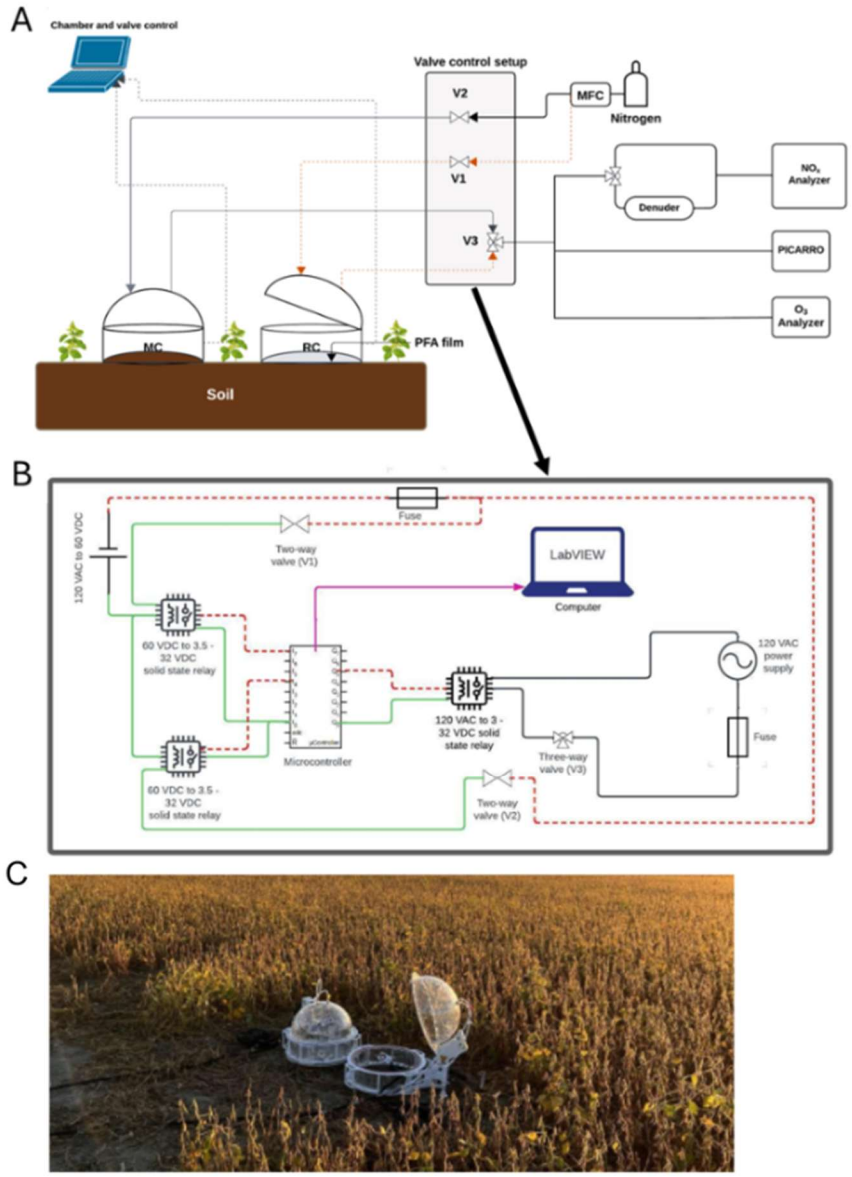

Figure 1. (**A)** Schematic of the dynamic chamber system to measure N_r and GHG fluxes. The components of the system include: the chambers, a dilution gas source (nitrogen (N_2) or zero air (ZA)), solenoid valve control, gas transfer lines, and gas analyzers. Grey lines indicate dilution gas flow from a source (e.g. cylinder) to the measurement chamber (MC) and air sampled from the MC to the analyzers. The dashed orange line represents these same flows relative to the reference chamber (RC). Communication lines from the chambers to a computer for automated control and ancillary sensor data collection using the chamber software (eoslink-AC; blue dotted lines). (**B**) The valve control setup for flow control in the complete dynamic chamber system, illustrating electrical components and lines needed for full automation using LabVIEW. It includes two 24 V DC two-way valves (V1 and V2; red dashed lines for negative electric potential, green for positive), with power supplied by solid-state relays, and a three-way 120 V AC valve (V3; black lines) with a power supply and another solid-state relay. The purple arrow represents the USB data acquisition connection from the microcontroller to a computer running the LabVIEW VI for valve control. (**C**) Field deployment of the dynamic chamber system, where the closed chamber is the reference and the open chamber functions as the measurement chamber.

The RC component of this system is designed to continuously baseline the physical interactions and chemistry happening on its surfaces both before and after quantifying reactive gas fluxes with the MC. Here, the flux measurements are made every 30 minutes, where one chamber is closed for gas analysis while the other is open to the ambient atmosphere. The sampling time interval was determined based on i) obtaining enough measurements at 1-minute time resolution to perform a reliable accumulation or loss linear regression, and ii) an ability to detect the lower limit of field HONO flux values previously reported in the literature for our pilot field study (see Section 2.7). For the first criterion, this includes an exclusion of the first and last few measurements (3 to 5) to allow complete gas replacement in the chamber lines and analyzers, as well as the disruption of the sealed environment when the chamber cycle alternates. The resulting accumulated mixing ratios of HONO at the lower literature limit in the chamber, closed for 30 minutes, are well above the 1.4 parts per billion (ppbv) mixing ratio detection limit (LOD) of even a modified NO_x analyzer (Crilley et al., 2023; Lao et al., 2020; Zhou et al., 2018; Nodeh-Farahani et al., 2021).

Headspace recirculation to facilitate analyte mixing ratio accumulation or depletion for non-destructive spectroscopic GHG analysis is a common measurement approach to decrease flux observation times. Reactive nitrogen measurements, in contrast, are typically destructive techniques that change the identity of the target analyte in the act of quantifying its abundance. To interface with such instruments, the sampled air needs to be replaced (Linde Canada Plc, PN: NI LC250-230) to balance the flow demand in a closed chamber. This balance is delicate even when

using mass flow controllers (MFCs) on both incoming and outgoing flows, and the best solution we identified is to provide a slight overflow that takes advantage of the chamber design to vent excess pressure through a short length (~15 cm) of 1/8" ID (3.175 mm), ¼" OD (6.35 mm) tubing that keeps the internal pressure equivalent to ambient. The flow differential between make-up gas and sampling is roughly 400 cm^3 min^{-1}. Such a supply of make-up gas was explored across a range of potential flow rates when using destructive gas analyzers (e.g., three instruments each sampling at 1 - 4 standard litres per minute, L min^{-1}) to find that 6 L min^{-1} is the upper limit of flow-through where the chamber pressure is not substantially perturbed from ambient and the chamber lid retains its seal.

In the field, a flux measurement cycle begins with closing the RC while the MC is open. At defined intervals, they alternate their open-closed states. Flows of make-up gas to each chamber are modulated with a pair of two-way solenoid valves. When sampling from the RC, one valve (V1; Figure 1) is open to permit make-up gas flow while the other valve (V2) is closed to prevent the flow from being directed to the MC. On the sampling lines, a three-way solenoid valve (V3) alternates to guide flow from whichever is closed to the suite of gas analyzers. All instrument and operational details are provided in Section 2.1.3.

2.1.2 Automated controls: system, data collection and processing

The chamber eosLink-AC software (Eosense Inc., Dartmouth, NS) is used to define the duration of chamber opening and closing cycles, and logs chamber temperature, pressure, and auxiliary sensor data associated with a given eosAC-LT chamber. Each chamber requires a 12 V DC power supply connected by USB to a laptop through a weatherproof communication cable, controlling the chamber lid and data transfer.

When a chamber cycle begins, a text file is generated and includes measurement time elapsed, chamber lid status, and sensor data. This data file is updated at least once every 10 seconds, varying between 2-8 second intervals, which we average onto a 1-minute time base to match measurements from the slowest gas analyzers. The solenoid valves are modulated by the electrical circuit shown in Figure 1B. Automation can be facilitated by a microcontroller (NI-6509i, National Instruments) programmed with a custom-scripted LabVIEW VI (LabVIEW version 2020). Further design information and full details of this sampling strategy and script can be found in Section S1 of the

Supporting Information and is available on the GitHub repository alongside our VI (https://github.com/fjs-vdblab/fluxchamber.git).

2.1.3 Instrumentation for N_r and GHG flux measurements

The mixing ratios of NO and NO_2 were measured using a commercially available chemiluminescent NO_x analyzer (EC 9841, American Ecotech, Warren, RI). The calculated LOD determined from sampling dry zero air was 0.84 ppbv, 0.67 ppbv and 1.07 ppbv for NO, NO_x, and NO_2 (or HONO when using the denuder as described below), respectively. The instrument has an operating range of 0 – 20 parts-per-million by volume (ppmv), a sample flow rate of 0.5 L min^{-1}, and reports measurements at a time resolution of 1 minute. To quantify NO_2, it is reduced to NO on a heated molybdenum catalyst (325 °C). To prevent interferences reported by others from atmospherically-relevant acidic species in this system (e.g. HONO, HNO_3, and N_2O_5) the sampled air from the chambers during field experiments was passed through a sodium carbonate (Na_2CO_3) coated annular denuder to reduce bias in the NO_2 measurement, as these species and other components of NO_y (e.g. peroxyacetyl nitrate; PAN) may also be reduced to NO (Villena et al., 2012). The Na_2CO_3 denuder was prepared according to the EPA Compendium Method IO-4.2 (Winberry Jr et al, EPA, 1999) to remove atmospheric acids by reactive uptake to the basic coating. As part of our controlled laboratory and pilot field study experiments, this denuder was also used to selectively measure HONO by scrubbing this target gas for a specified period, but it would include the other known interferences. If the NO_y term is depositing, it could include other NO_y detected by the same conversion mechanism, but if emitting we expect it to be dominated by HONO. Ideally, a platform like time-of-flight chemical ionization mass spectrometry (ToF-CIMS) would be used for disambiguation, but was not available at the time of this work.

A commercial O_3 analyzer (Serinus 10, American Ecotech, Warren, RI) was used to measure mixing ratios, quantify O_3 loss to surfaces, and constrain the reaction of O_3 with NO to form NO_2 in the pilot study sampling. This analyzer employs a non-dispersive UV absorption cell to quantify O_3 in the sampled air. The calculated LOD from sampling zero air is 0.95 ppbv at 1 minute time resolution, with an operating range of 0 to 20 ppmv and a sampling flow rate of 0.5 L min^{-1}. Quality control procedures for the NO_x and O_3 instruments can be found in Section S2.

The mixing ratios of the GHGs N_2O, CH_4, CO_2, H_2O, and NH_3 sampled from the automated chamber system were measured using a Picarro G2509 which uses cavity ring down spectroscopy. The analyzer has a time response of ~ 8 seconds for N_2O, CH_4, CO_2, H_2O and < 2 min for NH_3. It was used for the lab experiments and the pilot field study. The customized version of the instrument sampled at ~0.23 L min^{-1} and was equipped with an inlet filter. To minimize adsorption and chemical interactions of NH_3 on instrument surfaces, stainless steel gas handling components, including the inlet bulkhead, were replaced with PFA counterparts. The instrument cavity material was treated with a SilcoNert® coating by the manufacturer. We did not observe changes in its performance for the measured gases when operated according to the manufacturer guidelines. The Picarro G2509 analyzer spectroscopic mixing ratio determination means a full span calibration is not a regular necessity. Despite this, we validated its calibration and performed quality control checks in the lab to ensure the accuracy and stability of the analyzer for all aspects of this work (Section S2).

2.2 Chamber modifications to minimize NO_2 reactions on chamber surfaces

To transfer reactive gases through these chambers, interactions with surfaces need to be limited at all points of potential adsorptive or reactive losses. The custom-made base plate (Figure S1) was used to assess gas interactions on the commercial chamber surfaces. and identification of parts for replacement. First, the gas inlet and outlet push-to-connect fittings in the original configuration have plastic grips, with an internal component made of brass, which is informally known in the atmospheric chemistry community to have strong interactions with nitrogen oxides. These were replaced with PTFE Swagelok® bulkhead fittings (PN: T-400-1-4**;** Figure S2). Second, the polyacrylate wall and lid surfaces of the chambers had the 51 μm (0.002”) PFA film applied to the inner surfaces using double-sided tape to retain actinic transparency and PAR transfer to contained plants and surfaces (Figure S2).

2.3 Chamber modification validation using GHG and N_r gases

Before and after our modifications, we had to ensure that the non-reactive GHG transfer was unchanged in addition to challenge tests for the transfer of N_r gases. It was expected that N_r gases would interact and/or react on chamber surfaces that would differ between the unmodified and

modified variants and 15 m of standard PFA sampling tubing. Determining the time constants of fill (E1, E2) and decay (E3, E4) of these interactive and/or reactive gases in the chamber system allowed us to contrast their behaviour against that expected from a modelled theoretical inert trace gas in our system (Figure 2). Equations used to model mass transfer in our chambers were derived from Pape et al. (2009). The resulting accumulation curve was modelled by the theoretical function:

$$\mu_{fill}(t) = 1 - e^{-\left(\frac{t}{\tau_{fill}}\right)} \quad \textbf{(E1)}$$

$$\tau_{fill} = V/Q_{fill} \quad \textbf{(E2)}$$

Where μ_{fill} represents the normalized mixing ratio of gas in the chamber at a time (t, min) relative to the maximum mixing ratio within the measurement cycle, τ_{fill} is theoretical accumulation timescale for transfer of an ideal inert gas (min), V is the volume of the chamber (0.072 m^3), and Q_{fill} represents the total experimental flow rate (2 L min^{-1}). Similarly, the theoretical decay curve when emptying the chamber can be obtained, where τ_{emp} is the theoretical decay timescale for gas transfer (min) and Q_{emp} is again the total experimental flow rate (2 L min^{-1}).

$$\mu_{emp}(t) = e^{\left(-\frac{t}{\tau_{emp}}\right)} \quad \textbf{(E3)}$$

$$\tau_{emp} = \frac{V}{Q_{emp}} \quad \textbf{(E4)}$$

2.3.1 Instrumentation and materials for control experiments

Control experiments for the transmission of GHG and N_r gases were conducted by filling and emptying the chambers with known quantities at mixing ratios relevant to the atmosphere, as well as quantities expected to accumulate during real observations of modest emission fluxes (e.g. from a fertilized agricultural field). All assessments herein matched: the standard configuration of the chambers with all fittings, 15 m of ¼" O.D. (6.35 mm) PFA gas transfer tubing, flow rates, valves and gas transfer lines to instrumentation, with line/fitting/valve/instrumentation surfaces included. Details to control gas concentrations can be found in Section S3 of the SI.

2.3.2 Filling and emptying experiments with N_r, O_3, and GHGs

The positive control experiments filled the chambers in both modified and unmodified configurations and time constants were calculated from the measurements. In each filling experiment, the chamber was flushed with pure N_2 from a dewar (Linde Canada, PN: NI LC250-20) until a stable baseline level of each gas mixing ratio was reached; typically, these were values at the analyzer detection limits. Then, a blend of GHGs or one of the N_r analytes was delivered into the chamber with N_2 dilution at 2 L min^{-1}, which was sampled at 1.8 L min^{-1} by the analyzers (Figure S4). The gases were added to the chamber until the observed concentration (C) reached the known value being delivered (C_0), within error. Since different mixing ratios of the gases were added for these control experiments, normalized concentrations facilitate data analysis and visualization. Where surface interactions could be identified (e.g. for NH_3), the role of surfaces versus air exchange was explored using double exponential fits (see ES-1 and ES-2 in Section S3) (Crilley et al., 2023; Ellis et al., 2010; Moravek et al., 2019). The gases were emptied back to the initial baseline level before starting the next replicate or a new experiment with a different target gas. Time constants for filling and emptying were determined by fitting the observations in Igor Pro 8 (Wavemetrics, Portland, OR, US).

Similarly, the Eosense eosMX multiplexer is designed to coordinate chamber flux measurements using eosAC chambers with non-destructive analyzers, such that headspace can be recirculated while the chambers are closed. One of these devices was characterized following similar modifications. This system is appealing as it has the eosLink-MX software (Eosense, V1.9.07), for communication, scheduling actions, and logging peripheral data from all connected eosAC chambers. It features dedicated chamber tubing inlets and outlets, along with a COMM port supporting up to 12 eosAC chambers. Each chamber channel includes two Swagelok gas fittings for transport to analyzers and for recirculating, or in the case of N_r measurements, supplying a dilution gas to the chamber headspace.

To optimize the performance for N_r species, the original stainless-steel (SS) Swagelok fittings and solenoid valves were compared against replacement PFA bulkhead unions (Swagelok, PFA-420-61), and a PTFE 3-way valve (Clippard, NR1-2-12-G2). A 2 L min^{-1} flow of dry zero air containing the target compounds was passed through the SS valve with SS fittings or the PTFE valve with PFA fittings for 30 minutes each. The flow was measured before and after the valves to ensure the

setup was free of leaks. The ratio of the transferred gas amount to the nominal identified surface interactions impacting downstream gas analyzers. Details are presented in Sections 2.7 and S4.

2.4 Characterization of NO_2 and O_3 loss on chamber surfaces

Losses of NO_2 in the chamber were characterized by addition of 5-10 ppbv NO_2 under relevant relative humidity (RH) conditions (45-85% RH; Figure S5; Section S5). The NO_2 mixing ratio and RH range covered for these experiments are representative of the ambient atmosphere in an urban area (Toronto North Station, ECCC). The experiments were performed progressively and in triplicate with 5 ppbv of NO_2 and 85% RH, starting from the unmodified configuration of the chamber, replacement of fittings, and covering the inner surface with PFA film to quantify their efficacy in minimizing NO_2 loss and/or transformation on chamber surfaces. These were followed by varying NO_2 mixing ratios and RH to characterize the dependencies in the modified system.

Quantification of NO_2 and HONO in the chamber air was done using the alternating solenoid setup depicted in Figure S5. The sampled air is switched between two channels – one directly to the NO_x analyzer and the other through a Na_2CO_3-coated denuder – modulated every 5 minutes by a three-way solenoid valve (Fluoroware Galtek 1/4" F-NPT 3-way solenoid valve, 115V, PN: 203-3414-415. Entegris Inc., MN, US). When the sampled air flows directly to the analyzer, the total mixing ratio of NO_2 and acidic NO_y species, like HONO and HNO_3, is measured and has been termed NO_2^* (Crilley et al., 2023; Lao et al., 2020; Zhou et al., 2018). When the flow is directed through a Na_2CO_3 denuder, it selectively scrubs HONO and HNO_3, leaving behind NO_2 (Possanzini et al., 1983). Under the controlled NO_2 composition used in our experiments, it is expected that HONO will be the only acid present in the sampled air, as such experimental systems have been thoroughly characterized by Finlayson-Pitts et al. (2003), and HNO_3 is retained on the surfaces (R3) (Barney & Finlayson-Pitts, 2000; Huang et al., 2002; Kamboures et al., 2008). As a result, by the differential measurement of mixing ratios recorded in the two channels (E5) every 5 minutes, HONO can be quantified.

$$HONO = NO_2^* - NO_2 \quad \textbf{(E5)}$$

To quantify the amount of NO_2 lost to the chamber surface relative to the mixing ratio of NO_2 added to the chamber during an experiment, the NO_2 loss fraction (f_{NO2}) was found to be informative for mass balance between the two processes.

Similarly, we tested the modifications and aging of the installed PFA film surfaces on O_3 transfer. It is among the most sensitive/reactive species to transfer and is expected to drive reactive loss of NO when measuring N_r fluxes. The fraction of O_3 lost to chamber surfaces was quantified from 150-250 ppbv using a clean and unmodified chamber with PTFE bulkhead fittings replacing the push-to-connect brass fittings (Section S5).

The fraction of O_3 lost to chamber surfaces was then quantified in duplicate on a modified chamber with the interior chamber surfaces covered by brand new PFA film or one exposed to ambient air for more than two years, with 15 days of continuous use in an agricultural field during our pilot study.

2.5 Proof of concept N_r fluxes from agricultural soils

2.5.1 Soil sample N_r emissions for lab experiments

Randomized soil samples weighing 4-5 kg were collected into Ziploc® bags from an eight-plot grid established at an agricultural field site in Lambton County, ON, Canada (43°09'36.0" N 81°55'48.0" W). The samples were used to investigate emissions in the lab with and without the addition of fertilizers. Individual and pooled samples from the plots were used. Bulk soil samples were prepared for lab-based chamber measurements by removing debris, roots, and seeds, followed by drying at 35 °C for 24-72 hours on a stainless-steel mesh tray covered with aluminum foil, to prevent alteration of the microbial community from exposure to unrealistic temperature regimes. After drying, samples were stored in Ziploc® bags at room temperature until use.

Ultrapure water (18 MΩ·cm; Milli-Q®, Sigma-Aldrich, St, Louis, US) was added to approximately 350 g of a dry soil sample to achieve ~28% volumetric water content (VWC). The soil sample was loaded into the chamber on a foil-lined tray, and the water content was measured using a soil moisture probe inserted fully into the sample (TEROS 11, VWC range for mineral soils: 0.00 – 0.70 m^3/m^3; accuracy: ± 0.03 m^3/m^3; resolution: 0.001 m^3/m^3, METER Group Inc., WA, USA). Zero air modified to 65% RH was delivered at 3.6 L min^{-1} to the chamber headspace where the soil was contained. The soil started the drying process from a VWC of approximately 25% with the flows held constant for around 4 days or until the VWC reached 15%. The chamber was sealed to conduct the drying cycle while our modified NO_x analyzer and the Picarro G2509 measured fluxes. Unamended soil samples and others fertilized with urea ($CO(NH_2)_2$), ammonium carbonate (AC, $(NH_4)_2CO_3$), ammonium bicarbonate (ABC, NH_4HCO_3) at mass surface densities

of 100 kg N ha^{-1} were assessed. A similar experiment was conducted with ammonium nitrate (NH_4NO_3) at the same fertilizer mass surface density using only the modified NO_x analyzer. These fertilizer application values are at the upper end of those used in North American and European agriculture at present. Soil VWC and headspace RH were recorded using auxiliary sensors within the chamber.

2.5.2 Field deployment of automated dynamic N_r chambers

The RC and MC setup was deployed to make automated N_r flux measurements from the same agricultural field as in the prior section. The observations took place in early September 2022 at the end of a soybean (*Glycine max*) cropping season. A detailed description of the campaign and its results is the subject of a separate work, so we only provide a brief overview here. The total measurement period was approximately two weeks in duration to test system performance. Generally, conditions were hot and dry, without precipitation, and the soybeans surrounding the observed soils were undergoing senescence during the measurement period. The chambers were deployed only on the soil, between crop rows, and operated to quantify fluxes as outlined in Section S7. After an initial 7-day period of observing baseline fluxes from the field, an experimental perturbation was conducted to stimulate N_r emissions through the addition of an aqueous urea solution equivalent to 22 kg N ha^{-1} of fertilizer added by broadcast application, followed by washing into the soil by an equivalency of 2.5 cm (1") of rain depth. The modified NO_x analyzer and the Picarro G2509 were used to measure the N_r and GHG fluxes continuously.

2.6 Soil flux determination

The flux of a gas is the rate at which it is transferred across an interface (e.g., soil to atmosphere) per unit area per unit time. Gas fluxes are of high interest in agriculture as they give insight into the uptake or emission of N-bearing gases that may alter fertilizing effects. They are also important for assessing the state of plants or soils at interfaces through metrics like primary productivity, in which case measurement of a GHG like CO_2 provides the insight (Anthony & Silver, 2024; Li et al., 2016; Okiti et al., 2025). The RC captures environmental fluctuations such as temperature or pressure change and directly observes the interactions of ambient gases with surfaces within the sampling setup (i.e. chambers, gas transfer lines, valves, and analyzers), as well as tracking reactions, allowing for corrections to every net flux (F_{net}) measurement cycle (E6 for reactive gases and E7 for non-reactive gases, as derived in Section S7).

$$F_{\text{net}} = (\lambda).\left(\frac{V}{A}\left(\frac{\Delta C_m}{\Delta t_m} - \frac{\Delta C_r}{\Delta t_r}\right) + \frac{Q_{\text{out}}}{A}\left(\frac{\int_{t_{1m}}^{t_{2m}} c_m(t)\ dt}{\Delta t_m} - \frac{\int_{t_{1r}}^{t_{2r}} c_r(t)\ dt}{\Delta t_r}\right) - \frac{V}{A}\left(\frac{\int_{t_{1m}}^{t_{2m}} R_m(t)\ dt}{\Delta t_m} - \frac{\int_{t_{1r}}^{t_{2r}} R_r(t)\ dt}{\Delta t_r}\right)\right)$$

E6

Where V is the volume of the chamber (m^3), A is the surface area (m^2) enclosed by the chamber and governing the gas flux; Q_{out} is the volumetric flow rate of air exiting the chamber ($m^3\ s^{-1}$); $c_m(t)$ and $c_r(t)$ are target gas concentrations within the MC and RC (mol m^{-3}), respectively; $\frac{\Delta C_m}{\Delta t_m}$ and $\frac{\Delta C_r}{\Delta t_r}$ represent their corresponding rates of change (mol $m^{-3}\ s^{-1}$); and F_{net} is the resulting net gas flux per unit area (mol $m^{-2}\ s^{-1}$).The terms R_m and R_r denote the instantaneous chemical production or loss rate expressed in units of mol $m^{-3}\ s^{-1}$ for consistency. The dimensionless attenuation factor λ is required to correct for interactions of reactive gases with surfaces. Such surface interactions, which are particularly strong for gases like NH_3, significantly reduce the measured rate of concentration change within the closed chamber (Figure 4). Thus, λ is derived as the ratio between a theoretical unattenuated gas (i.e. an inert GHG like N_2O) and the observed target gas concentration from controlled deliveries. These are then integrated over the chamber closure interval (Section S7). This term has the surface effects from chambers, gas transfer lines, and analyzers embedded by definition and must be determined empirically for any configuration. The attenuation correction reduces bias and improves the accuracy of flux estimates.

$$F_{\text{net}} = \lambda \cdot \frac{P_{\text{air}}}{R \cdot T} \cdot \left(\frac{V}{A}\left(\frac{\Delta X_m}{\Delta t_m} - \frac{\Delta X_r}{\Delta t_r}\right) + \frac{Q_{\text{out}}}{A}\left(\frac{\int_{t_{1m}}^{t_{2m}} X_m(t)\ dt}{\Delta t_m} - \frac{\int_{t_{1r}}^{t_{2r}} X_r(t)\ dt}{\Delta t_r}\right)\right)$$

E7

For inert gases (E7)**,** the fluxes can be based on mixing ratios, where $X_m\ and\ X_r$ are the gas volumetric mixing ratios (mol X per mol air), P_{air} is the air pressure (Pa), T is the absolute temperature (K), and R is the universal gas constant ($J\ mol^{-1}\ K^{-1}$). By comparing the RC and MC observations, the effects of specific environmental conditions on N_r (E6) or GHG (E7) exchange fluxes can be isolated, while accounting for surface effects and chemical transformations in the former.

3 Results

3.1 Determining time constants of reactive nitrogen and GHGs

The time constants of both filling and emptying the chambers were calculated using concentrations normalized to their initial values, for each N_r gas and GHG. These were used to quantify gas transfer times through the chambers and to confirm performance relative to theory. Where departures were identified, we quantified the extent of surface interactions for the various target analytes so corrections for determining in situ fluxes could be implemented (Table 1, Figure 2).

3.1.1 Time constants of greenhouse gases (GHGs)

Determination of the GHG time constants benchmarks the chamber performance before and after modifications. In both configurations CO_2, CH_4, and N_2O were anticipated to behave as non-reactive trace gases with little to no physical interactions on chamber surfaces.

The theoretical fill and empty rates for the chambers with a flow rate of 2 L min^{-1} are 36 min. The average measured time constants of filling for CH_4, CO_2, and N_2O in the unmodified chamber were 37 ± 1 min, 37 ± 2 min, and 37 ± 1 min, respectively (Table 1). During emptying, they were 37 ± 1 min, 37 ± 1 min, and 38 ± 2 min, respectively. These measurements are not different from theory within the limits of experimental accuracy (Figure 2). Since the GHGs are effectively transferred through both the modified and unmodified configurations of the chamber, the baseline performance of the chambers was not affected by the hardware modifications. Therefore, comparison with the time constants of N_r gases provides a description of their interaction or transformation processes on the modified chamber surfaces.

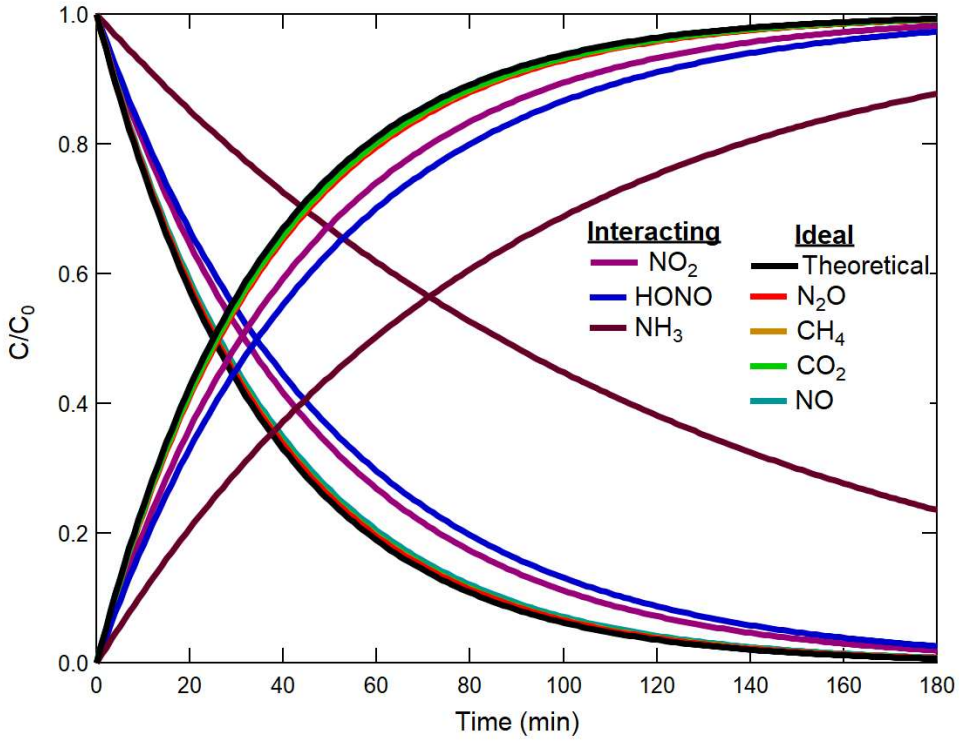

Figure 2. Addition of N_r and GHGs to a modified dynamic chamber. For clarity, the coloured traces show the fitting curves corresponding to the response time in concentration normalized to the delivered value of each gas while filling and emptying the chamber. The black trace corresponds to a perfect non-reactive transfer of an ideal trace gas based on volume transfer in the chamber only. Note that the N_2O, CH_4, CO_2, and NO fill and empty traces all overlap with the theoretical fill and empty curves.

3.1.2 Time constants of reactive nitrogen gases

In the modified chamber, the time constant of filling or emptying with NO was 38 ± 1 min. The obtained value is similar to GHGs, as NO is not expected to have strong surface interactions. The slower time response of the NO_2, HONO, and NH_3 measurements results from two processes: (1) the exchange of the sample air volume in the gas transfer lines and the chamber, and (2) the adsorption and desorption of the gas onto and from their surfaces (Whitehead et al., 2008). Increases in the extent of surface interactions followed the increasing polarity, reactivity, and/or ionizability of gases in the order of NO_2, then HONO, and most for NH_3 (Figure 2).

For example, NO_2 is lost more readily than NO, possibly through its known reaction on surfaces to make HONO and HNO_3, being lost itself in the process (Finlayson-Pitts et al., 2003). It also has

547 higher water solubility than NO, but lower than for HONO or NH_3. Similarly, a decrease in
548 transmission efficiency for HONO could be explained by its weakly acidic nature (pKa of 3.16)
549 (Finlayson-Pitts et al., 2003) and solubility in water (Henry's law constant of 0.48 mol m^{-3} Pa^{-1};
550 (Schwartz & White, 1981)) that facilitate partitioning and dissociation in surface water films,
551 which could generate non-volatile nitrite (NO_2^-) on chamber surfaces. This chemistry will slow
552 the transfer of gas-phase HONO through the chambers, as the NO_2^- would need to protonate before
553 being lost as neutral HONO when repartitioning to the gas phase (R4, R5). Finally, NH_3 has the
554 most delayed transmission, likely because it undergoes strong inter-molecule interactions and
555 ionization on the chamber surfaces and/or with any interfacial water (Henry's law constant of
556 $5.9x10^{-1}$ mol m^{-3} Pa^{-1} (Orkin et al., 2011); pKa of 9.25 (Lide, 2009)). The same interactions on
557 tubing surfaces and potential partitioning into the tubing material may also occur before reaching
558 the analyzer (Pagonis et al., 2017). The best improvement between the modified and unmodified
559 configurations was 2.6 ± 2.5 min for HONO, with smaller improvements observed for NO_2 and
560 NH_3 during the filling process. Improved time constants when emptying N_r from the chambers had
561 similar trends (Table 1). As a result, increasing delays from NO through NH_3 exist in our N_r gas
562 suite due to increasingly stronger interactions with chamber surfaces and gas handling lines.

563 The determined surface interaction values (D; Table 1; ES-2, Section S3) demonstrate the expected
564 greater impact of surfaces when no reactive gas is present in the headspace prior to filling, and a
565 lesser effect during emptying as the exposed surface has equilibrated with the analyte, which is
566 commonly referred to as passivation. For NH_3 specifically, the fill has a D value of 89%, while
567 during emptying it is only 23%, similar to our findings with NH_3 transfer for other N_r instruments
568 (Crilley et al., 2023). The surface interactions for these gases are minimized in the modified
569 chambers to facilitate more time-efficient measurements of surface exchange. However, they
570 necessitate the use of the λ term when deployed in the MC-RC configuration for those N_r species
571 which experience partial transmission, such as NH_3. The λ term is required to obtain accurate
572 values, as the enclosed flux measurement surface should be perturbed for the least amount of time
573 possible when making field measurements, and the chambers cannot be closed for several hours
574 to allow surface-active gases to passivate the lines. One potential option to improve the system
575 performance further for NH_3 could be to heat the gas transfer lines between the chambers and gas
576 analyzers. In addition, minimizing the potential for transformations reduces the frequency required
577 for in-field characterization of these processes through positive and negative gas delivery controls.

For NO_2, specifically, we sought to quantify this as a function of modifying components of our chambers, as NO_2 is the most reactive gas in our suite (Section S5).

Table 1. Summary of time responses for addition and removal of GHGs and N_r gases at 2 L min^{-1} in unmodified and modified chamber configurations. Time response for a theoretical fill or empty e-folding time is 36 minutes. Where analytes were observed to undergo surface interactions, a double exponential fit was used, with the first time constant representing the known gas exchange rate of 36 minutes, and the second time constant reported (*) alongside an assessment of the magnitude of surface interactions through the D-value (%; Section S3) (Crilley et al., 2023; Ellis et al., 2010; Moravek et al., 2019). Variability shown is one standard deviation of the mean from replicate experiments (n=3).

Gas species	Direction	Unmodified (min)	Modified (min)	Improvement (min)	D (%)
NO	Fill	38.8 ± 0.7	37.8 ± 0.6	1.0 ± 0.7	-
	Empty	37.9 ± 1.5	36.0 ± 0.6	1.9 ± 2.1	-
NO_2	Fill*	18.9 ± 0.6	18.0 ± 3.1	0.9 ± 3.2	94 ± 18
	Empty*	21.2 ± 1.2	20.4 ± 1.4	0.8 ± 1.9	78 ± 21
HONO	Fill*	21.9 ± 1.1	19.3 ± 1.2	2.6 ± 1.6	74 ± 10
	Empty*	23.2 ± 1.4	21.2 ± 0.9	2.0 ± 1.7	71 ± 9
NH_3	Fill*	69.6 ± 0.4	68.2 ± 0.5	1.4 ± 0.6	89 ± 3
	Empty*	76.9 ± 0.8	75.0 ± 4.6	1.9 ± 4.7	23 ± 4
CO_2	Fill	37.9 ± 1.5	37.0 ± 1.8	0.9 ± 2.3	-
	Empty	38.0 ± 1.8	37.0 ± 1.2	1.0 ± 2.2	-
CH_4	Fill	37.9 ± 1.1	36.8± 1.2	1.1 ± 1.6	-
	Empty	39.1± 1.7	37.2 ± 1.2	1.9 ± 2.1	-
N_2O	Fill	38.6 ± 2.1	36.7 ± 1.2	1.9 ± 2.4	-
	Empty	39.7 ± 1.3	37.7 ± 1.6	2.0 ± 2.1	-

3.2 Multiplexer modification impacts on gas transfer

The multiplexer (eosMX; Eosense Inc.) allows operation of up to twelve dynamic chambers simultaneously with a suite of gas analyzers. However, it is constructed with stainless steel (SS) valves and fittings that would be expected to facilitate strong interactions and/or losses of target gases in the N_r analyte suite. Valves and fittings made of SS have a higher tendency to chemically interact and/or adsorb reactive gases compared to fluoropolymer replacements. To address this uncertainty, the gas transfer efficiency as a percentage loss in the multiplexer versus a bypass line was evaluated specifically for NH_3 and NO_2, alongside standard GHGs as they passed through fittings and gas handling solenoid valves made of SS or PFA and PTFE replacement parts.

The loss fractions were modest and measurable when using minimal lengths of PFA tubing (~50 cm) instead of the standard 15 m gas transfer lines. The most substantial loss was observed on SS, as expected due to its known tendencies (Vaittinen et al., 2014). When the GHGs were delivered for 30 minutes, typical of a chamber closure period in the field, their losses ranged from 10% for N_2O to 19% for H_2O. Meanwhile, NO_2 exhibited 17% loss on the SS surfaces, and the greatest effect was seen for NH_3 with a loss of 38% (Figure S6). In contrast, losses on the chemically inert and hydrophobic surface of the PFA fittings and PTFE valve were negligible (<1%) for most gases, except for NH_3, which still exhibited a measurable loss of 11%. Other reports have also shown up to 15% loss of NH_3 at atmospheric pressure on PTFE and PFA surfaces (Ellis et al., 2010; Shah et al., 2006; Vaittinen et al., 2014). While it is expected that the SS would eventually passivate and improve the transmission of the GHGs in a standard recirculation approach, this is not likely to be the case for destructively analyzed N_r and even more so if it facilitates a chemical transformation. Replacing the multiplexer SS valves and fittings with PFA fittings and PTFE valves provided a 9–27% reduction in surface losses of N_r compounds and GHGs. We strongly recommend the use of PTFE and/or PFA materials over SS for more accurate measurement of N_r species when interfacing the dual chamber setup with the destructive N_r analyzers needed for field flux measurements, whether using a custom setup or the commercially available multiplexer.

3.3 Minimizing NO_2 losses and determining controlling variables

In addition to the rate of transfer of N_r gases, chamber modifications are necessary to prevent reactive losses. These experiments determined the magnitude of NO_2 lost to chamber and gas transfer tubing surfaces due to chemical and/or physical transformations, and demonstrate the

effectiveness of the chamber modifications in minimizing these losses. For NO_2, a probable chemical transformation pathway is its heterogeneous conversion to HONO (R3), which is favourable under atmospherically relevant humidities, and the resulting water-adsorbed surfaces are expected to exist throughout the chamber and sampling lines.

3.3.1. Chamber modification impacts on NO_2 losses

Substantial reduction in NO_2 loss fraction (f_{NO2}) and transformation was observed from the implemented PFA and PTFE modifications under conditions of 83% RH and 5 ppb of NO_2. In the original unmodified configuration of the chamber, f_{NO2} was 0.36 ± 0.02 (Figure S7) which was reduced to 0.22 ± 0.03 with the PFA film, a relative decrease of 18%. This is consistent with the acrylic chamber surfaces and fasteners to the chamber frame facilitating physical and/or chemical loss of NO_2.

The film of PFA, as with other fluoropolymers, is known to have excellent chemical resistance and low reactivity towards a range of chemicals, including NO_2 (Ebnesajjad, 2005). In addition, the superhydrophobic nature of these materials reduces the accumulation of water on surfaces, which can reduce the surface reaction of NO_2 (Finlayson-Pitts et al., 2002; Jenkin et al., 1988; Stutz et al., 2002) and analytical bias in the measurement of trace gases like HONO, especially when instrument gas sampling inlets do not take this into account (Crilley et al., 2019; Von Der Heyden et al., 2022).

The replacement of the brass-lined push-to-connect bulkhead fittings with PTFE led to a similar decrease in f_{NO2}, which was reduced by 17% to a final value of less than 0.05 ± 0.02 (Figure S7). These fitting surfaces act as the largest surface-driven NO_2 loss despite their surface area being very small compared to that of the entire chamber configuration and with a very small contact time against the gas sample (0.012 s per fitting at a flow rate of 2 L min^{-1}).

The loss of NO_2 in the commercially available system is challenging to attribute solely to the heterogeneous hydrolysis reaction. During the characterization experiments, the conditions inside the chamber were matched to those reported by previous lab studies, which have shown that high RH, presence of NO_2, and surface adsorbed water on surfaces favour this loss mechanism (Jenkin et al., 1988; Stutz et al., 2004). The reaction is known to occur on surfaces such as Pyrex (Jenkin

et al., 1988) and borosilicate glass (Finlayson-Pitts et al., 2002), but no prior studies to date, nor this study, have demonstrated metallic surfaces as facilitating this mechanism.

The inert PTFE fittings dramatically minimized transformations, while PFA film lining the inner chamber surfaces was also effective, but less so. Our results indicate that water-adsorbed and metallic surfaces, such as brass, facilitate substantial loss and/or transformations of NO_2. Further investigation is required to confirm the mechanism(s) at play and is beyond the scope of this work.

3.3.2. RH-facilitated NO_2 loss as a function of concentration

A complete characterization of f_{NO2} and the amount of HONO in the fully modified chamber was determined across a range of environmentally relevant RHs and NO_2 concentrations. We found that the absolute and fractional NO_2 losses were highest under the highest RH conditions (85%; Table 2). However, the f_{NO2} does not appear to follow a concentration-dependent trend across the additions made at lower RHs, with at most 0.4 ppbv NO_2 lost across the remainder of the tests, a value which is equivalent to the LOD of the NO_x analyzer used. This would generate 0.2 ppbv of HONO according to the disproportionation of the hydrolysis mechanism, which is well below the analyzer detection limits. The modifications successfully reduced NO_2 losses below 10% across all environmentally relevant conditions the chambers are expected to encounter, with our findings here suggesting that the mass lost is nearly constant and independent of NO_2 mixing ratio at RHs below 85%, while being marginally higher at and above this value.

Quantifying f_{NO2} and the amount of HONO made in the chamber is required for the correction of field datasets. The dual chamber system, via the RC, can also quantify any changes in these processes over time if standard additions to the headspace are conducted. Consequently, important parameters such as NO_2 deposition fluxes on surfaces can be better estimated (Pape et al., 2009).

Since the inferred HONO mixing ratios from the chamber surfaces across various environmental RHs are nearly invariant at 0.2 ± 0.1 ppbv, it is simple to background correct any observational datasets by subtracting this amount from the total HONO measured in the chamber. In addition, as the NO_2 values expected in most atmospheric gas samples during field measurements are well into the ppbv range (>3.3 ppbv per 30-minute flux measurement for a 0.08 μg N m^{-2} hr^{-1} emission), the

corrections would be easy to implement in post-processing of datasets and have minimal impact on the technical aspects of the analytical determinations.

Table 2. Characterization of NO_2 lost in the modified chamber across environmentally relevant ranges of NO_2 and RH. The loss fraction (f_{NO2}) and HONO produced in the chamber were quantified. Variability (±) provided is one standard deviation of the mean from replicate experiments (n=3).

RH (%)	NO_2 added (ppbv)	NO_2 lost (ppbv)	f_{NO2}	HONO produced (ppbv)
85	5	0.50 ± 0.01	0.1 ± 0.02	
85	7	0.70 ± 0.04	0.1 ± 0.02	
85	10	0.50 ± 0.07	0.05 ± 0.01	
65	5	0.30 ± 0.10	0.06 ± 0.02	
65	7	0.40 ± 0.09	0.06 ± 0.02	<1.1[a]
65	10	0.30 ± 0.08	0.03 ± 0.01	
45	5	0.30 ± 0.05	0.05 ± 0.01	
45	7	0.40 ± 0.04	0.06 ± 0.00	
45	10	0.30 ± 0.08	0.03 ± 0.01	

[a] – below instrument detection limit of 1.1 ppbv determined as S/N=3 while sampling zero air

It should be noted that the amount of HONO in the chamber was below the LOD of the NO_x analyzer for HONO (1.1 ppbv), meaning that the upper limit of HONO inferred may perhaps, in fact, be negligible. Therefore, future experiments that wish to detect small N_r fluxes accurately will need to focus on reproducing these experiments with a higher performance instrument, such as a time-of-flight chemical ionization mass spectrometer (ToF-MS) or long-path absorption photometer (LOPAP), which have lower detection limits (Crilley et al., 2019; Lee et al., 2014; Neuman et al., 2016; Reed et al., 2016).

3.3.3 Loss of O_3 with and without fluoropolymer modifications

Ozone loss was observed in both modified and unmodified chamber configurations, with 18% lost to clean 15 m PFA lines alone when transferring 30 ppbv. The unmodified chambers lost 45% across delivered mixing ratios spanning 150-250 ppbv. This was reduced to 35% when the fluoropolymer modifications were implemented. When the PFA film was aged by 15 days of ambient sampling and 2 years of exposure to lab air, the losses were substantially exacerbated, reaching 80%. Such outcomes are expected and can be attributed to several factors discussed in detail in Section S5, primarily involving surface reactions with built-up films of deposited organics, adsorption, and material interactions (Burkholder et al., 2015; Ebnesajjad 2017; George et al., 2015; Plake et al., 2015). We recommend regular replacement of the PFA film as part of the N_r system maintenance, coupled with quality control procedures to characterize material performance for target gases.

3.3 Proof-of-concept reactive nitrogen fluxes using soil samples in the lab

Proof-of-concept flux measurements were performed using the modified dynamic chamber system to demonstrate that emissions of N_r gases from agricultural soil samples can be measured under controlled conditions, similar to many prior reports using custom-built soil chambers (Almand-Hunter et al., 2015; Pape et al., 2009; Tang et al., 2019, 2020).

3.3.1. Fluxes of NO, NO_2, and HONO from agricultural soil samples

Emission fluxes were measured from two pooled and two individual soil samples collected from a single agricultural field (Table 3; Section S6). The average and integrated fluxes of N_2O, NH_3, NO, NO_2, and HONO were assessed under controlled, environmentally realistic (65 % RH), drying conditions (Table 3).

As the soils dried, NO and NO_2 emissions increased, with NO fluxes highest across all replicates and reaching up to 2.50 μg N m^{-2} hr^{-1}. This trend is consistent with the prior work of other researchers, showing peak NO emission potentials when VWC drops below 25% during soil drying, which is when microbial nitrification and denitrification processes are suggested to become more active (Bao et al., 2022; Oswald et al., 2013). The soil VWC at which these maxima occur can vary depending on soil type, texture, and microbial diversity therein (Ludwig et al., 2001;

Schindlbacher et al., 2009). Plot-level replicates from our field had a higher integrated NO flux (i.e., > 2600 μg N m^{-2}), compared to the pooled replicates (<1000 μg N m^{-2}), likely indicating real differences in preserved microbial hotspots, intact plot-level soil aggregates, true spatial variability, and plot-specific N availability (Table 3). Soil texture and aggregate size, for example, play an important role in building the porous structure of soil, which has implications for the release of gases (Mangalassery et al., 2013). Soil aggregates, therefore, govern the release of gaseous N_r analytes like NO based on the aerobic or anaerobic state of the soil. Here, our low level of soil manipulation (i.e. not ground, no sieving) will drive some of the variability by preserving these features, which exist across and within real soil systems (Lipiec et al., 2007). Individual plot samples also retain plot-specific microbial communities when working with intact soil, whereas soil grinding can temporarily inhibit microbial activity. While we tried to minimize soil handling and processing extremes in these experiments, a measure of homogeneity was also pursued, and fully intact soil cores were not assessed.

Integrated NO_2 fluxes showed the same trend, with more sample-to-sample variability as one pooled replicate (R2) produced over three times the emissions of R1, despite both experiments being conducted across identical moisture content ranges (Table 3). Given the limited studies directly measuring NO_2, such as Purchase et al. (2023), this variability is difficult to interpret and highlights the need for more assessments of its production pathways and controls, which our developed chambers show promise for.

The observed average HONO fluxes remained low across all of the samples, ranging from 0.05 to 0.25 μg N m^{-2} hr^{-1} (Table 3). These values are lower by more than an order of magnitude compared to those reported in other controlled laboratory studies, where HONO fluxes exceed 900 μg N m^{-2} hr^{-1} (Oswald et al., 2013; Su et al., 2011; Wang et al., 2021). These discrepancies are concerning, given recent emphasis from the scientific community on the atmospheric impacts of soil-derived HONO on air quality. Here, the results from our agricultural soil samples may reflect the differences in our methodology, such as the soil handling and preparation steps prior to and during experiments. Many prior reports prepare their samples in ways that strongly deviate from real-world conditions (e.g. initial soil drying temperatures above those occurring under ambient conditions, extreme storage conditions, grinding, sieving, use of dry zero air to flush chambers, etc.). Further drivers of variability within the category of heavily altered soil samples from the

literature include pH, NO_2^- availability, and NH_4^+ or NO_3^- content, all of which are known to influence biotic and abiotic HONO formation pathways (Wu et al., 2019).

Our HONO fluxes from the agricultural soil samples studied here are consistent with field observations under ambient conditions, where average emissions have been reported to largely remain below 7.2 μg N m^{-2} hr^{-1} (Tang et al., 2019; Xue et al., 2024). This does suggest that greater care in sample preparation, and likely also a widely agreed-upon standard procedure, is needed to study soil HONO emissions relevant to atmospheric models.

The integrated HONO fluxes for the pooled replicates yielded 185 μg N m^{-2} and 146 μg N m^{-2}, respectively. From the individual sample replicates, which were slightly wetter than the pooled, the integrated HONO fluxes were 690 and 739 μg N m^{-2}, which was unexpected because the overall moisture regime accessed by the pooled soil experiments was not lower than those from the plot samples. The drier soils would have been expected to yield greater integrated HONO emissions (Oswald et al., 2013), yet this was not the case. Additional replicates and experimental controls, while beyond the scope of this study, would allow further attribution of the controls over the observed HONO variability.

Table 3. Average and integrated fluxes of NO, NO_2, and HONO (in μg N m^{-2} hr^{-1} and μg N m^{-2}, respectively) from agricultural soil samples across two soil VWC ranges. Both the average and integrated fluxes were calculated over a constant period within the noted range of soil VWC. Values are reported as mean ± standard error.

Soil sample	Soil VWC Range (%)	Duration (hr)	Avg Flux (μg N m^{-2} hr^{-1})			Integrated flux (μg N m^{-2})		
			NO	NO_2	HONO	NO	NO_2	HONO
Pooled R1	16-22	125	1.0 ± 0.04	0.05 ± 0.02	0.06 ± 0.02	2400 ± 120	160 ± 50	190 ± 50
Pooled R2	16-22	125	1.0 ± 0.04	0.20 ± 0.02	0.05 ± 0.01	2500 ± 130	500 ± 60	150 ± 40
Plot R1	22-27	65	1.2 ± 0.05	0.40 ± 0.03	0.20 ± 0.02	3400 ± 150	1300 ± 90	690 ± 70
Plot R2	22-27	65	1.0 ± 0.03	0.50 ± 0.04	0.30 ± 0.02	2600 ± 100	1600 ± 100	740 ± 50

These findings demonstrate the utility of the modified custom-built dynamic chambers for accurately capturing N_r fluxes under controlled laboratory settings, but they also highlight the need for more such systems to be implemented across the scientific community to better consider both biogeochemical soil properties and environmental context when interpreting the impacts of N_r fluxes obtained in the lab and scaling them to real soils. There seems to be potential for skewing the atmospheric impacts as a result, in particular for HONO, as the standard approaches have been designed to replicate NO fluxes (Behrendt et al., 2014). Most global models do not consider the effect of soil HONO on air quality through O_3 production and oxidation chemistry. Several modelling studies, like Ha et al. (2023) and Tian et al. (2024), have incorporated the order of magnitude or higher HONO fluxes reported from lab studies, like those by Su et al. (2011), Wang et al. (2021), Oswald et al. (2013), and Meusel et al. (2018). They estimated significant HONO production with maximum flux potentials of 830 μg N m^{-2} hr^{-1}, 95 μg N m^{-2} hr^{-1}, 70 μg N m^{-2} hr^{-1}, and 55 μg N m^{-2} hr^{-1}, respectively. In contrast, the field observations that do exist suggest that real HONO fluxes are much smaller at 2-17.5 μg N m^{-2} hr^{-1} (Song et al., 2023; Tang et al., 2019). Similarly, Wu et al. (2022) have used the regional WRF-Chem model to explore the impact of soil HONO emissions on the concentrations of atmospheric HONO, OH, and O_3.

Agricultural soil HONO emissions have been suggested to significantly contribute to OH radical production, accounting for approximately 10% to 60% of total OH formation in rural areas before noon (Oswald et al., 2013; Su et al., 2011), which often exceed the contributions from O_3 photolysis. Additionally, high HONO emissions from agricultural soils have been reported to increase local O_3 concentrations by ~0.5 - 1.0 ppb in low-NO_x rural environments where VOCs are not limiting (Zhang et al., 2021), with even greater impacts observed during fertilization periods (Wu et al., 2022). Modelling studies, using GEOS-Chem and CMAQ, for example, claim that incorporating soil HONO emissions improves the agreement between observed and simulated O_3 levels, particularly during the morning (Zhang et al., 2021).

Only a few studies have conducted estimates of soil NO_x emissions under reasonable conditions, like Bao et al. (2022) and Wu et al. (2022), where the researchers tried to mimic field conditions. Even in such an area that has been long studied, large uncertainty still exists around soil sources of NO_x, particularly for agricultural activities, where uncertainty is still at least ±30% due to limitations in lab characterizations and field experiments (Gong et al., 2025). It is not surprising,

804 then, that a similar issue exists for the very recent work on HONO soil emissions. The NO_x
805 uncertainty range results from intricate soil biogeochemical processes and varies with crop types,
806 soil texture, fertilizer types and application rate (Gong et al., 2025). This longstanding and
807 established difficulty in predicting soil NO_x for use in global chemical models means that doing
808 so for HONO without careful ground truthing of real-world emissions could lead to substantial
809 inflation of the impacts on atmospheric chemistry and air quality. Care should be taken in using
810 HONO emissions from lab studies in global models, as it seems they pose a risk of overestimating
811 their atmospheric impacts until a more representative experimental design can be obtained with
812 chamber systems like the one used here.

813 **3.3.2 Fluxes of N_r from fertilized agricultural soil samples**

814 Agricultural soils amended with chemical fertilizers are expected to be hotspots for NH_3, N_2O,
815 HONO, and NO_x emissions. Here, we demonstrate the use of our developed chambers to measure
816 these analytes under controlled lab conditions using our lightly processed pooled soil samples and
817 four fertilizers: urea, ammonium nitrate (AN), ammonium bicarbonate (ABC), and ammonium
818 carbonate (AC) with the temperature maintained at 23 °C, VWC between 25–29%, and headspace
819 RH held at 65% for three days, simulating realistic atmospheric and environmental N_r flux
820 exchange conditions following farm field fertilization (Figure 3). In all experiments conducted
821 with the Picarro G2509, the mixing ratio of N_2O began to rise approximately four hours after the
822 experiment started. In the example shown for urea, it peaked at 0.79 ppm after 12 hours, which
823 was followed by a gradual decline (Figure 3a). This pattern likely reflects the incubation period of
824 nitrifying and denitrifying bacteria that leads to the subsequent release of gases like HONO, as
825 depicted in Wang et al. (2021), and N_2O in Liu et al. (2022). In contrast, the mixing ratio of NO
826 remained relatively constant throughout the three days (Figure 3b), with NO_2 increasing as the
827 N_2O emissions decreased (Figure 3c). In this example experiment, no measurable emissions of
828 HONO were detected despite the substantial presence of urea and evidence of active microbial
829 nitrification and denitrification from the other emitted gases (Figure 3d). Lastly, the urea
830 application example in Figure 3e shows the expected significant NH_3 emissions, with the
831 integrated amount reaching 22% of the applied N over the three-day incubation period. These
832 findings are consistent with our existing knowledge that NH_3 volatilization as an N loss mechanism
833 dominates early N_r losses from fertilizers.

Volatilization of NH_3 is well-characterized as a major pathway for N loss from fertilizers (Behera et al., 2013; Govoni Brondi et al., 2024; Liu et al., 2020; Moravek et al., 2019; Pan et al., 2016, 2022; Paulot et al., 2014). Besides agronomic concerns due to N loss and reduced fertilizer efficiency related to NH_3 emissions from fertilized soil (Anas et al., 2020), it is a key precursor to secondary inorganic aerosols in the atmosphere with impacts on respiratory and ecosystem health, visibility, and climate (Dennis et al., 2010; Edwards et al., 2024; Fowler et al., 2013; González Ortiz et al., 2020; Jang et al., 2025; Seinfeld and Pandis, 2006).

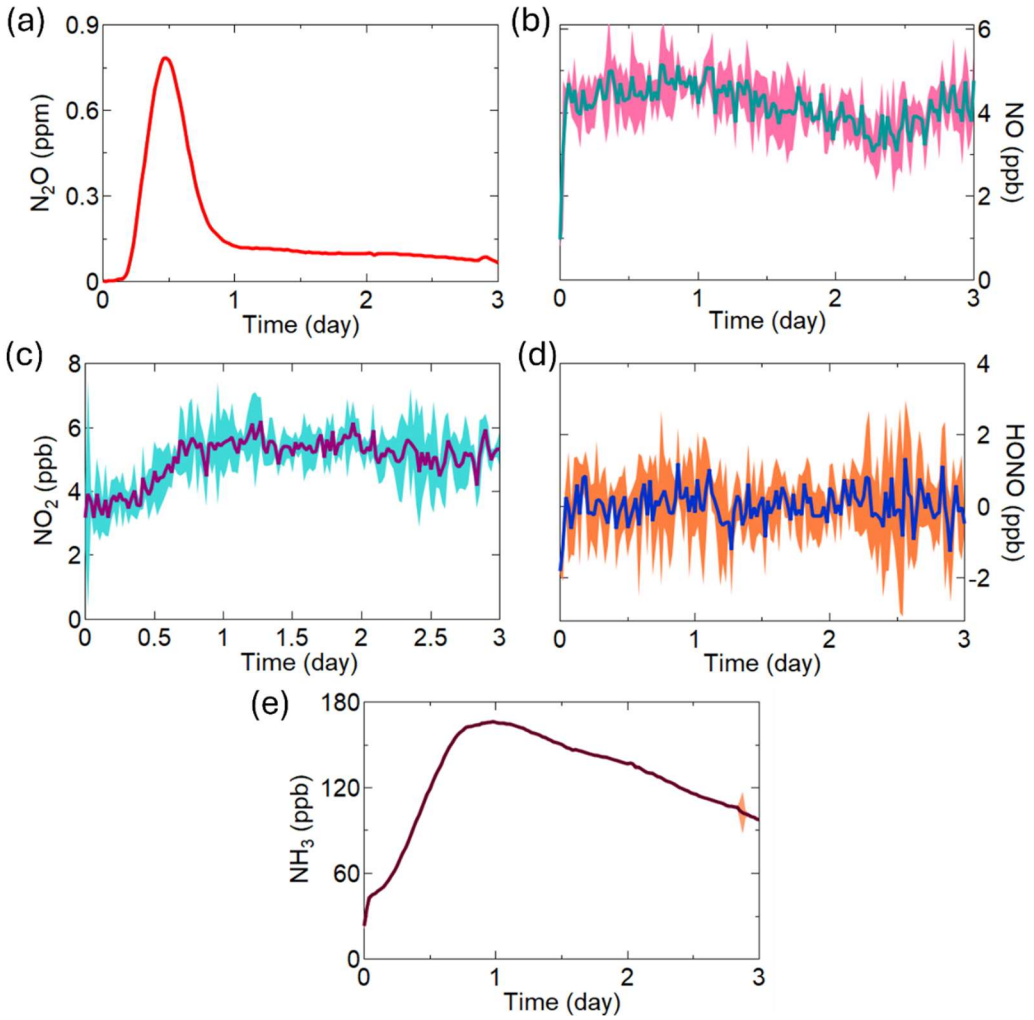

Figure 3. Soil emissions of the comprehensive N_r suite from soil treated with urea, including (a) N_2O; (b) NO; (c) NO_2; (d) HONO; and (e) NH_3. The NO, NO_2 and HONO emissions were measured at 1-minute resolution and averaged to 30 min. The standard deviation (±2σ) around these averages is shaded around the main trace. Similarly, the 2-second resolution of N_2O and NH_3 measurements were also averaged to 30-minute intervals with ±1σ provided in shading.

Emissions of NH_3 and N_2O were observed to be far greater in terms of integrated amounts from the fertilized samples (Figure 4). Integrated flux for NH_3 produced by soil treated with ABC accounted for 77% of total N_r flux (i.e., 85 900 μg N m^{-2}), followed by AC, which was 63 700 μg N m^{-2}. This is not surprising, since the use of chemical fertilizers increases the concentration of NH_4^+ in the soil that can deprotonate to emit neutral NH_3 and, in the presence of ammonia-oxidizing microorganisms, increase the production of N_2O (Luo et al., 2025). Nitrous oxide released from the addition of urea accounted for the highest integrated flux of 32 400 μg N m^{-2} observed, representing 89% of total N_r released, followed by 25 300 μg N m^{-2} and 9 600 μg N m^{-2} for ABC and AC, respectively. One way that has been proposed to reduce these large N_2O emissions from inorganic fertilizers is to change the application form to organic fertilizer, as the NH_4^+ in soil is produced more slowly (Luo et al., 2025). Due to a limited duration of access to the G2509 to conduct this work, we were unable to measure the N_2O and NH_3 emitted from unamended soils or those treated with AN. Regardless, based on the obtained data, the values found here are similar to those observed under real environmental conditions (Figure 4). For our sample without N amendment, the integrated flux of NO was the largest (2 400 μg N m^{-2}; 87% of total NO_y), followed by comparable levels of NO_2 (160 μg N m^{-2}) and HONO (190 μg N m^{-2}). The fluxes of NO_x and HONO were below 1 μg N m^{-2} hr^{-1} for all the nutrient addition treatments, suggesting a similar trend as those observed under field conditions and from our lab results with unamended soils (Figure 4, Table S1, Section S6). The exact mechanism behind the HONO release, being due to nitrification and/or denitrification, cannot be definitively assigned based on flux data alone, and many factors drive these emissions. There are discrepancies still observed between HONO flux measured from the treated soil samples in the laboratory and similar measurements in literature (Oswald et al., 2013; Su et al., 2011), some of which report fluxes of up to ~3 600 μg N m^{-2} hr^{-1} and are likely overestimating the soil N_r fluxes found in the real world. In contrast, our results are in close agreement with the field-based measurements of Tang et al. (2020), which also used a dynamic chamber flux method.

These in-lab experiments show that simultaneous speciated N_r emissions directed towards mass balance analysis in a controlled environment can be conducted using a single chamber and potentially applied to an array of chambers, as others have done for a subset of gaseous N_r (Scharko et al., 2015; Tang et al., 2019). With the limited replicates we explored here, our results raise a

question for researchers who have been using lab studies as a standard to predict and incorporate HONO soil emission values, particularly for regional and global models.

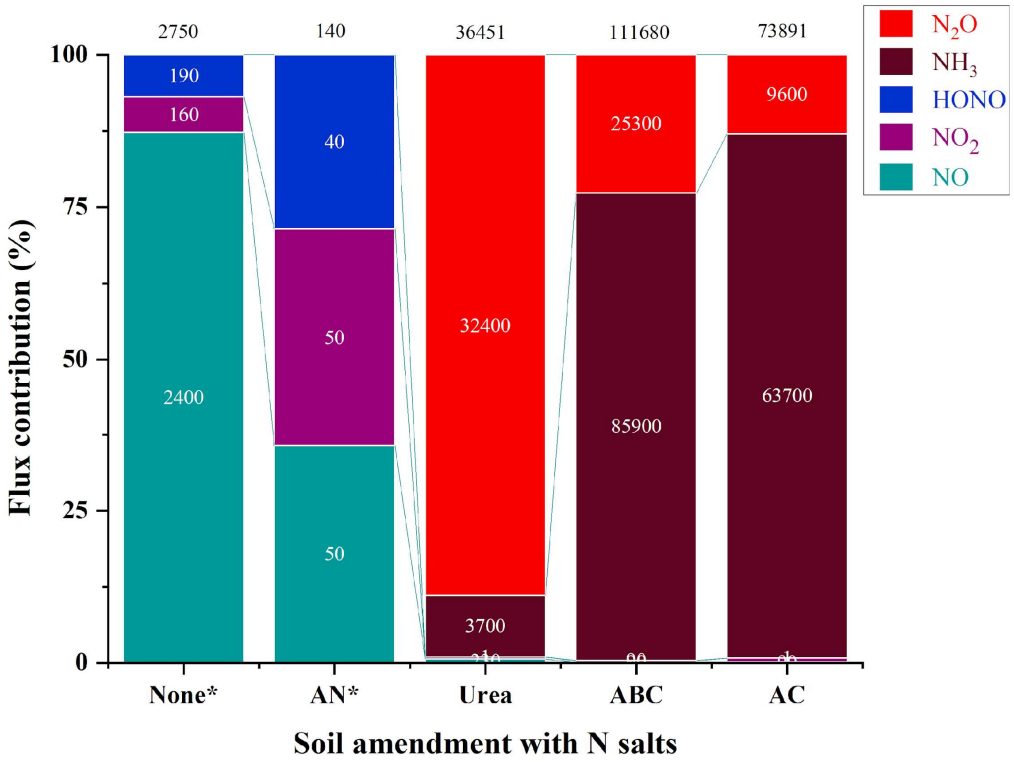

Figure 4. Relative flux contribution of soil treated with four different N-containing fertilizer salts. Each segment shows the proportion of integrated flux of NO (cyan), NO_2 (purple), HONO (blue), NH_3 (brown) and N_2O (red), with discrete flux values presented in white text, and the total flux provided in black text above the column (μg N m^{-2}). Some samples (denoted by *) were only characterized for fluxes of NO, NO_2 and HONO using the modified NO_x analyzer, as the duration of our access to the G2509 for NH_3 and N_2O measurements was limited.

3.3.3 Dual chamber field deployment for automated continuous dynamic fluxes

A pilot scale field campaign was carried out to demonstrate the application of our dual soil flux chambers in capturing N_r gas exchange processes. A paired MC-RC setup was deployed in the same field a year after the soil samples were collected for our lab experiments. During a period of stimulated N_r emission from an in situ experimental application of urea, the mixing ratios of NO, N_2O, and NH_3 were impacted compared to the unfertilized state. The changes within both the MC and RC were measured and used to calculate fluxes (Figure 5). The purpose of Figure 5 is methodological to demonstrate how rate, dilution, and reaction terms combine in the observed rates of concentration change during chamber cycles. The selected data for NH_3 correspond to

measurements taken after the fertilization event, while the selected NO and N_2O data segments are examples for separate observation times which best demonstrated the contributions of all terms before the fertilization event. Taken together, these three separate examples for the mathematical terms contributing to the net flux in E6 and E7 can be considered more easily – they are entirely ascribed to the rate term otherwise. Each set of observations spans three consecutive hours of dynamic changes in gas concentrations within the chambers, which allow fluxes to be calculated. For the 0.5 Hz measurement rate of the Picarro, it is clear from the accumulation and depletion of target gases in Figure 5 that a shorter observation period than 30 minutes could be used when high time resolution instrumentation across all target species is available. The benefit of this would be to reduce both the alteration of the composition of the chamber headspace and diverging physical conditions between the chamber and ambient environment, ultimately obtaining better flux estimates. However, for this pilot study, the 1-minute time resolution of the NO_x analyzer and the method for determining HONO by difference with an annular denuder every 5 minutes required a 30-minute interval. A shorter closure period could also have the drawback of worse flux detection limits when fluxes are small, and more variability due to a less robust regression of the accumulation or depletion rate. For example, this would increase the value of λ for NH_3 (Figure S11; Section S7) and its relative error (4% for a clean system, Section S7.3) as well as other surface-interacting gases.

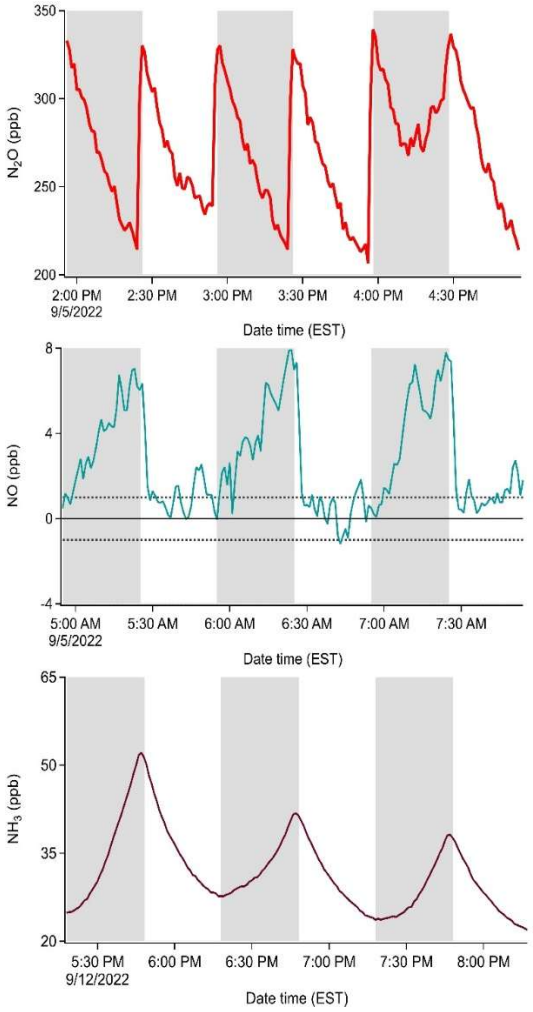

916

917 **Figure 5.** Mixing ratios of N_2O (ppb), NO (ppb), and NH_3 (ppb) in the MC (grey shading) and RC
918 (unshaded) from three consecutive cycles during the pilot field study. Cycles are shown for
919 representative, non-simultaneous periods to illustrate term contributions. The NH_3 cycles
920 correspond to measurements taken after the fertilization perturbation, while the NO and N_2O
921 cycles are earlier, before fertilization. The dashed lines for the NO measurements indicate ±1 ppb
922 (3σ noise), where the positive boundary represents the detection limit of the NO_x analyzer.

923

924 The breakdown of the flux components for NH_3, N_2O, and NO can allow the contributions of the
925 experimental setup (e.g. dilution) and environmental factors (e.g. reaction) to be considered
926 independently (Figure 6). We consider these across a consecutive triplicate of flux determinations
927 from the pilot field deployment, to provide meaningful examples. The uncertainty in each term is
928 estimated from the variance between the triplicate of consecutive MC and RC observations,
929 through the measured slopes (i.e. using E6 or E7) and assumes that ambient atmospheric
930 composition did not change substantially during this error derivation period.

The rate term (dC/dt) is the dominant contributor to the determined flux for all three gases (Figure 6), which are all positive and indicate emissions despite their clearly differing temporal trends. Each contribution term is defined and discussed in further detail in Section S7. Accurate quantification of trace gas fluxes using dynamic chamber systems requires correction for attenuation caused by surface interactions. These effects can significantly suppress the measured accumulation rate of reactive species within the closed MC (Figure 5). To account for this, the attenuation factor (λ) was introduced in this work (ES12), defined as the ratio of the theoretical concentration signal for an inert gas (e.g. as in our fill/empty experiments) to the measured signal over the chamber closure period. The value of λ is gas-specific and time-dependent, reflecting wall affinity and kinetics. This correction reduces flux bias, independent of chamber-specific losses. The highest attenuation was observed for NH_3, for which a λ of 5.40 was determined empirically for the 30-minute closure period. Comparative values for NO_2 and HONO are also provided in Section S7.3.

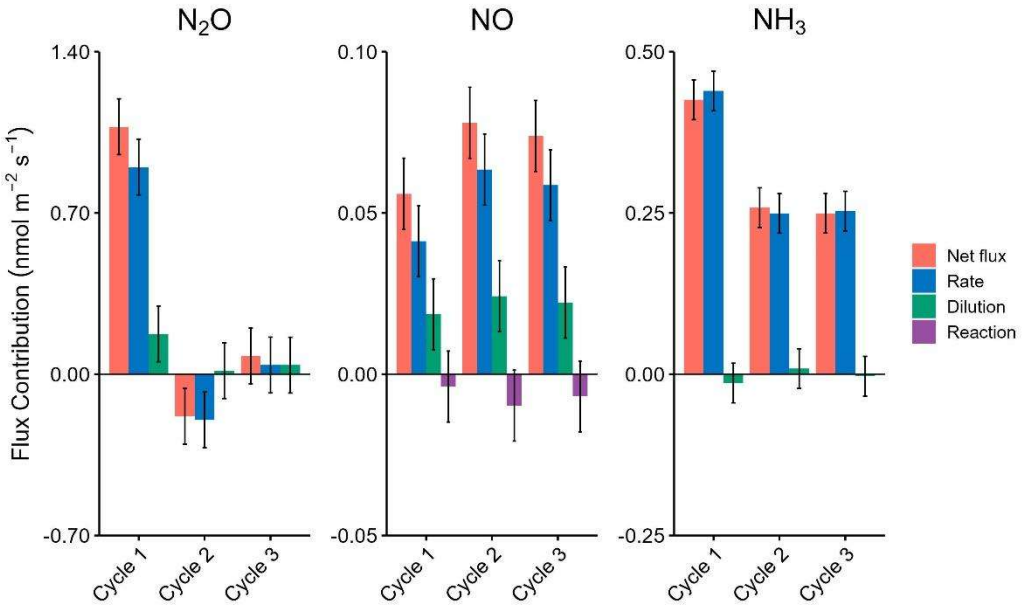

Figure 6. Contributions of different terms (rate, dilution, and reaction) to the net flux of NO, NH_3, and N_2O across three consecutive cycles (nmol m^{-2} s^{-1}). The rate represents the change in concentration measured over time, the dilution represents the integrated loss to dilution, and the reaction represents the contribution of known reactions happening inside the chamber. Error bars are calculated using the standard deviation about the mean of the corresponding terms from three consecutive chamber cycles. For visual clarity, the attenuation correction (λ = 5.40) for NH_3 is not applied in this figure, as it constitutes a linear scaling factor across all NH_3 bars (Section S7.3).

For N_2O, the first cycle exhibits the highest flux (1.07±0.12 nmol m^{-2} s^{-1}), while the second cycle showed uptake by the soil (-0.18±0.12 nmol m^{-2} s^{-1}), and the final cycle showed no net flux within error (0.08±0.12 nmol m^{-2} s^{-1}). This occurs for a non-reactive greenhouse gas like N_2O despite the concentration decreasing with time for both the measurement and reference periods, as the rate of decrease during the measurement cycle is slower than that from dilution in the RC alone (Figure 6). Across the three cycles, the rate of concentration change term contributed 84±15% to the measured flux in the first cycle, 109±98% in the second cycle, and 50±171% in the third cycle. The negative rate of concentration change in all of the observation periods arises due to the use of N_2O-free purge gas delivered to the chamber headspace, which is required for the gas sample to be destructively quantified, while not introducing ambient air into the chamber (Figure 5). This simultaneously prevents sudden changes in local outdoor air composition from making small fluxes difficult to detect, as well as reduces the uncertainty in the fluxes assigned. Here, the dilution terms range from 8 to 50% of the net flux, as would be expected from the N_2O exchange switching from emission to deposition during the three-cycle example (i.e. 3 hours). In the final measurement cycle, the rate of concentration change transitions from a loss to steady state during the observation period, suggesting that an instant of 'hot spot, hot moment' emission of N_2O was likely occurring. As such, the transition leads to no net flux for the observation period, which is a limitation of our dual-chamber approach compared to one with recirculating headspace, or that of an EC approach that can capture higher temporal resolution changes in concentration. The N_2O fluxes observed here are consistent with those reported for European arable soils using both dynamic and static chambers, where event-driven N_2O peaks after fertilization commonly range between 0.2 and 2.4 nmol m^{-2} s^{-1}, and background periods can be as low as 0.08 nmol m^{-2} s^{-1} (Kong et al., 2025, Murphy et al., 2022, Maier et al., 2024, Manco et al., 2025). Field-scale EC studies, such as Maier et al. (2022), have captured post-harvest pulses up to 1.6 nmol m^{-2} s^{-1}, highlighting the capacity of EC to resolve large, rapid emission events that single-point chamber systems may miss. However, dynamic chamber systems provide high-precision, temporally resolved flux data under controlled conditions, enabling direct attribution of emissions to specific soil management or environmental factors (Butterbach-Bahl et al., 2013; Kong et al., 2025). This makes dynamic chambers, like those demonstrated here, especially valuable for mechanistic and process-level studies.

For NO, the only gas we consider in the examples here with a reaction term, the reaction contribution is the smallest among the three flux components. Over all three cycles, the reaction

term opposed the net flux by less than 13%. The magnitude of the reaction term is always negligible, remaining within the ± 0.01 nmol m^{-2} s^{-1} variability caused by background correction from the RC. Instead, the time rate of change in concentration term drove 74–81% of the total flux for all three cycles and dilution accounted for the remaining 30–33%. The reaction term falling within the uncertainty range of no contribution in all three cycles (e.g. -0.01±0.01 nmol m^{-2} s^{-1} in the second cycle, where it had the greatest potential), indicates that its contribution is less certain than the other flux components as it is driven by the presence of O_3, which is rapidly lost upon chamber closure. Overall, the low contribution of the reaction term suggests this process has a minor role in measured NO fluxes. In other, more polluted regions, such as the North China Plain and the Pearl River Delta, where summertime ambient O_3 concentrations range from 60 to 275 ppbv, the exceedances above 200 ppbv during pollution episodes (Wang et al., 2017) could make this term very important. As noted above, the PFA film on the chamber surface will change its properties with respect to O_3 transmission over time, highlighting the utility of the RC in tracking this because it is designed to accumulate or lose the same atmospheric compounds as the MC on all sampling surfaces.

The resulting emission fluxes of NO observed in these three cycles were 0.056-0.078 nmol m^{-2} s^{-1}, which are well within the range reported for agricultural soils in North America and Europe, such as Taylor et al. (1999) who observed -0.07-4.2 nmol m^{-2} s^{-1} in Canadian fertilized cropland, and Pape et al. (2009) and Almand-Hunter et al. (2014) who reported values of 0.05-4.0 nmol m^{-2} s^{-1}, using dynamic chambers in grass and cropland soils. Therefore, in the case of NO for this example, the variability in the fluxes is largely driven by real fluctuations in the rate term. This highlights the sensitivity of the total flux to changes in the rate of concentration change, and the precision of the method, as the uncertainty in the final fluxes here is on the order of 14%. Compared to the dynamic chambers reported by these prior studies, the RC in our dual-chamber system offers a clear advantage by directly correcting for baseline fluctuations and environmental drift that can confound single-chamber approaches. This is especially important for reactive gases such as NO, which are susceptible to rapid loss to O_3 and short-term background variability (Taylor et al., 1999). In comparison to EC or flux-gradient techniques, which integrate over larger areas but may underestimate true NO fluxes due to post-emission chemistry (Taylor et al., 1999; Plake et al., 2015), our approach yields high-frequency, process-resolving data ideal for mechanistic and plot-scale studies.

For NH_3, the rate of change term dominates the total flux, contributing 103 ± 10%, 97 ± 16%, and 101 ± 17% of the flux in cycles one, two, and three, respectively, while the dilution term contributes inconsequentially at -3 ± 7%, 3 ± 12%, and -1 ± 12% in the same three cycles, respectively. The resulting emission fluxes of NH_3 observed across these cycles ranged from 0.43 ± 0.03 nmol m^{-2} s^{-1} in cycle one down to 0.25 ± 0.03 nmol m^{-2} s^{-1} in cycle three. The relatively small contribution of the dilution term is consistent with the expectation that the RC and MC exhibit similar dilution effects. The relative uncertainty in the final NH_3 fluxes is 7% for cycle one, and 12% for cycles two and three. By comparison, relative uncertainties were 14% for NO and ranged from 15% to 171% for N_2O, reflecting the greater variability and lower precision associated with the smaller flux magnitudes for those gases.

Our observed NH_3 fluxes (0.25–0.43 nmol m^{-2} s^{-1}) are consistent with literature values for managed grass and croplands. For instance, Milford et al. (2009) reported bi-directional background fluxes from –3.8 to 2.5 nmol m^{-2} s^{-1} before cutting intensively managed grassland, with larger diurnal emissions up to 42 nmol m^{-2} s^{-1} after cutting and maxima up to 224 nmol m^{-2} s^{-1} following fertilizer application. Abdulwahab et al. (2025) observed highly variable fluxes in intensively grazed French grassland, ranging from –6.6 to 188 nmol m^{-2} s^{-1}, with short-lived maxima above 300 nmol m^{-2} s^{-1} after slurry application, though most measurements were at much lower magnitudes. Notably, accurate quantification of NH_3 fluxes in this system critically depends on the application of the chamber-specific attenuation factor λ (Section S.7.3; Figure S11). Without this correction, true NH_3 fluxes would be underestimated by more than fivefold. While the RC correction plays a role in the flux calculations, its impact on NH_3 is less pronounced than on N_2O, where the correction significantly alters the net flux direction (Figure 5; first cycle). Chamber-based approaches such as ours provide a key advantage for NH_3 over micrometeorological methods like EC, which are especially prone to high-frequency attenuation and chemical interferences for reactive gases. As shown in Moravek et al. (2019), even state-of-the-art closed-path EC systems may recover less than half (as little as 46%) of true NH_3 fluxes due to instrument limitations and turbulence losses. Challenges were also evident for REA, where Xu et al. (2010) found that turbulence and surface effects complicated flux interpretation in cropland. Related methodological considerations have also been noted in other contexts. Schlossberg et al. (2017) highlighted how airflow and canopy structure can influence chamber NH_3 fluxes in turf systems, underscoring the need for chamber methods that minimize such artifacts. In contrast, our dynamic

chamber system, with a chamber-specific λ correction and RC, enables robust, bias-corrected quantification of both low and episodic NH_3 fluxes, as well as clear partitioning of emission and dilution terms, even under highly variable field conditions.

4. Conclusions

In this work, we presented a dynamic chamber system for N_r flux measurements, developed for the first time through the modification of commercially available chambers by implementing two key changes: the use of PTFE fittings instead of original brass fittings and the installation of an inert PFA film, which retains their actinic transparency. These modifications provide a targeted methodology for other researchers to convert commercially available chambers into those capable of measuring N_r. The performance of these modifications was quantified through the rise and fall time constants of target gas concentrations, as well as a reduction in reactive losses. The time constants for the transfer of GHGs were not different from those of a theoretically inert gas and showed no change from the modifications. Improved transmission for the reactive and surface-active N_r species NO_2, HONO, and NH_3 targeted here ranged from 0.8 to 2.6 minutes. Further improvement for NH_3 might be obtained by integration of heated gas transfer lines between the chambers and gas analyzers. Similarly, a commercial chamber multiplexing unit with stainless steel valves and fittings replaced with PTFE and PFA, respectively, resulted in a 9–27% reduction in surface losses of N_r compounds.

Only NO_2 showed reactive loss in the system, and the loss fraction in the chambers in their unmodified configurations was up to ~36%. Losses were reduced to the gas analyzer detection limits (<10%) with the same fluoropolymer modifications when atmospherically relevant NO_2 and RH mixtures were introduced. Loss of O_3 was pervasive within chambers in both their modified and unmodified configurations at 35% and 45% respectively, demonstrating the necessity of the RC. It allows characterization of deposited surface film reactivity for O_3, which is needed to account for the conversion of NO to NO_2 during a sampling period. The modified commercial system is capable of measuring dynamic soil fluxes of GHGs and N_r when MC and RC are deployed simultaneously.

Proof of concept flux measurements were conducted using real agricultural soil samples in the lab, with a single chamber, and during a pilot study in the field with a MC-RC pair. The lab soil emissions were found to be consistent with prior field reports in the literature for NO and HONO, with unexpected emissions of NO_2 also observed. Substantial variability in NO_2 and HONO emissions between replicates demonstrates the potential heterogeneity of soil emissions that may result from samples kept intact and subject to minimal preparation conditions. Upon the addition of typical fertilizers, like urea, substantial NH_3 and N_2O emissions fluxes matched expectations, with increasing quantities of NO, NO_2, and HONO as the soil water content decreased.

Last, fully automated operation of the chambers was carried out in a field pilot study with the delivery of external fertilizer conducted at the midpoint of the two-week period to stimulate N_r emissions, mainly in the form of NH_3. Continuous flux observations were made by switching sample flows between the RC and MC with a custom-built valve system to obtain continuous N_r fluxes. While the details of the entire campaign will be presented in a future manuscript, it was shown here how the developed measurement technique yields reliable flux determinations by accounting for known reactions and our lab-derived surface effects. The mathematical foundation of each term and its error in a mass balance equation, which are central to reducing flux bias, are fully described.

The duration of the chamber closure for the modified NO_x analyzer used in this work made a 30-minute observation necessary to obtain sufficient measurements for a reliable flux determination. Use of higher time resolution gas analyzers can readily reduce the observation period and continue to produce reliable fluxes, depending on the flux detection limit desired, and tolerance for inflated surface effects. One key limitation of the dynamic chamber approach is the limited surface footprint covered when it is notoriously known to be heterogeneous, and where EC and REA flux approaches are less susceptible to this effect. Using a multiplexer and a larger array of dynamic chambers, it is possible to reduce the susceptibility of the dynamic chambers to this issue. Similarly, the actinic transparency of the acrylic lid blocks UV photons, potentially limiting photochemical mechanisms of production for HONO. If paired with EC or REA, these chambers could be capable of quantifying the magnitude of these mechanisms for the first time. One further limitation is that the chamber and gas transfer line surfaces may accumulate material and change the mass transfer of gases, particularly NH_3, over time. This effect can be monitored using the

reference chamber if sufficient quantities are present in the ambient air, via the dilution decay rate and characterized in situ by a standard addition of the necessary gases to the headspace.

Through our modifications and validation, this work provides insight into how commercial dynamic chamber options, like those offered by Eosense, can be modified easily for scientists from various disciplines interested in studying N_r exchange at atmospheric interfaces. This is particularly important for research groups which currently do not have the expertise and resources to develop their own N_r flux measurement systems. The modified system utilizes destructive sampling techniques, as opposed to the re-circulation of chamber air, enabling integration of the dynamic chamber approach with various standard gas analysis instruments (e.g., NO_x chemiluminescence) to study their exchange. The large footprint allows gas concentrations to change in easily determined quantities even for very small fluxes. We show here, for the first time, that such a system can provide simultaneous measurement of NO, NO_2, HONO, NH_3, CO_2, H_2O, CH_4, and N_2O fluxes. In addition, we show fully automated operation of the chambers, switching of sample flows, and data collection workflows for continuous and unattended measurements of fluxes at field sites. Ideally, modern instrumentation like the ToF-CIMS would be coupled with this system to shorten the chamber closure duration and better distinguish HONO from other NO_y fluxes, instead of using a modified NO_x analyzer. Given the pressing need to understand global perturbations to the biogeochemical cycle of N, reduce nitrogen use in agriculture, and gauge the impacts of N status on biodiversity or ecosystem function, wider accessibility of N_r flux techniques for the global research community is needed to increase the pace of research outcomes and improve the capacity for interdisciplinary work between atmospheric and earth system researchers.

Data Availability: Data is available upon request from the Corresponding Author.

Competing Interests: TCV received supporting in-kind funds for this work from Eosense, Inc. and Picarro as it is mandatory in the NSERC Alliance Missions programme funding structure which facilitates research partnerships between the academy and industry. NN, CC, and SE are employed by Eosense, Inc.

Author contributions: TCV designed and oversaw the experiments, acquired funding, wrote parts of the manuscript, and guided writing and revision of all sections of the manuscript. MS wrote the

manuscript and performed all the lab experiments. KZA carried out the multiplexer experiments, conducted data analysis for the fill-empty experiment, provided guidance and feedback on the derivation of the mass balance flux model, and assisted in the revision of the manuscript. DF conducted some of the field measurements, worked up the pilot field study results and derived the dual chamber mass balance flux calculations, and made contributions to the writing and revision of the manuscript. LRC helped design the experiments, modify the chambers, write the LabVIEW code, conduct the pilot field measurements, and contributed to manuscript preparation and revision. AM contributed to the initial chamber lab setup and revision of the manuscript. FS performed some fill-empty and NO_2 loss experiments, designed the custom valve switching system, modified LabVIEW code for the pilot field measurements, and contributed to initial drafts of the manuscript. YEI and TH assisted with the GHG fill-empty experiments, YEI supported the pilot field study, and both contributed to manuscript revision. NN, CC, and SE provided technical support with setting up and modifying the chambers and multiplexer.

Acknowledgements: We gratefully acknowledge the support of Picarro for facilitating use of the G2509 analyzer during the chamber characterizations, lab experiments, and pilot study components of this work. The team at Shawnasey Farms Ltd. provided access to storage and machinery to install the experimental agricultural site for the pilot project, helped with daily campaign logistics, and the collection of soil samples.

Financial Support: All components of this work were supported by funding to TCV by the Natural Sciences and Engineering Research Council (NSERC) Alliance Missions program (ALLRP 570577-2021), with additional support from the NSERC Discovery Grants and Early Career Launch programmes (RGPIN-2020-06166 and DGECR-2020-00186). MS and YEI were supported by Ontario Graduate Scholarships, and MS was further supported by a Charles Hantho Award in Atmospheric Chemistry and the Enbridge Graduate Student Award.

5. References

Abdulwahab, M. O., Flechard, C., Fauvel, Y., Häni, C., Jacotot, A., Graux, A.-I., Edouard, N., Buysse, P., Viaud, V., and Neftel, A.: Aerodynamic gradient flux measurements of ammonia in intensively grazed grassland: temporal variations, environmental drivers, methodological challenges and uncertainties, EGUsphere [preprint], https://doi.org/10.5194/egusphere-2025-1605, 2025

Almand-Hunter, B. B., Walker, J. T., Masson, N. P., Hafford, L., and Hannigan, M. P.: Development and validation of inexpensive, automated, dynamic flux chambers, Atmos. Meas. Tech., 8, 267–280, https://doi.org/10.5194/amt-8-267-2015, 2015.

Anas, M., Liao, F., Verma, K. K., Sarwar, M. A., Mahmood, A., Chen, Z. L., Li, Q., Zeng, X. P., Liu, Y., and Li, Y. R.: Fate of nitrogen in agriculture and environment: agronomic, eco-physiological and molecular approaches to improve nitrogen use efficiency, Biol. Res., 53, 47, https://doi.org/10.1186/s40659-020-00312-4, 2020.

Aneja, V. P., Blunden, J., Claiborn, C. S., and Rogers, H. H.: Dynamic Chamber System to Measure Gaseous Compounds Emissions and Atmospheric-Biospheric Interactions, in: Environmental Simulation Chambers: Application to Atmospheric Chemical Processes, Springer, Dordrecht, 97–109, https://doi.org/10.1007/1-4020-4232-9_7, 2006.

Anthony, T. L. and Silver, W. L.: Hot spots and hot moments of greenhouse gas emissions in agricultural peatlands, Biogeochemistry, 167, 461–477, https://doi.org/10.1007/s10533-023-01095-y, 2024.

Bao, F., Cheng, Y., Kuhn, U., Li, G., Wang, W., Kratz, A. M., Weber, J., Weber, B., Pöschl, U., and Su, H.: Key Role of Equilibrium HONO Concentration over Soil in Quantifying Soil–Atmosphere HONO Fluxes, Environ. Sci. Technol., 56, 3960–3969, https://doi.org/10.1021/acs.est.1c06716, 2022.

Barney, W. S. and Finlayson-Pitts, B. J.: Enhancement of N2O4 on Porous Glass at Room Temperature: A Key Intermediate in the Heterogeneous Hydrolysis of NO2?, J. Phys. Chem. A, 104, 171–175, https://doi.org/10.1021/jp993169b, 2000.

Becciolini, V., Leso, L., Fuertes Gimeno, E., Rossi, G., Barbari, M., Dalla Marta, A., Orlandini, S., and Verdi, L.: Nitrogen loss abatement from dairy cow excreta through urine and faeces separation: The effect of temperature and exposure period on NH3 fluxes, Agric. Syst., 216, 103898, https://doi.org/10.1016/j.agsy.2024.103898, 2024.

Behera, S. N., Sharma, M., Aneja, V. P., and Balasubramanian, R.: Ammonia in the atmosphere: A review on emission sources, atmospheric chemistry and deposition on terrestrial bodies, Environ. Sci. Pollut. Res., 20, 8092–8131, https://doi.org/10.1007/s11356-013-2051-9, 2013.

Behrendt, T., Veres, P. R., Ashuri, F., Song, G., Flanz, M., Mamtimin, B., Bruse, M., Williams, J., and Meixner, F. X.: Characterisation of NO production and consumption: New insights by an improved laboratory dynamic chamber technique, Biogeosciences, 11, 5463–5492, https://doi.org/10.5194/bg-11-5463-2014, 2014.

1196 Benedict, K. B., Prenni, A. J., Carrico, C. M., Sullivan, A. P., Schichtel, B. A., and Collett, J. L.:
1197 Enhanced concentrations of reactive nitrogen species in wildfire smoke, Atmos. Environ.,
1198 148, 8–15, https://doi.org/10.1016/j.atmosenv.2016.10.030, 2017.

1199 Burkholder, J. B., Cox, R. A., and Ravishankara, A. R.: Atmospheric Degradation of Ozone
1200 Depleting Substances, Their Substitutes, and Related Species, Chem. Rev., 115, 3704–
1201 3759, https://doi.org/10.1021/cr5006759, 2015.

1202 Butterbach-Bahl, K. and Dannenmann, M.: Denitrification and associated soil N2O emissions due
1203 to agricultural activities in a changing climate, Curr. Opin. Environ. Sustain., 3, 389–395,
1204 https://doi.org/10.1016/j.cosust.2011.08.004, 2011.

1205 Chiaravalloti, I., Theunissen, N., Zhang, S., Wang, J., Sun, F., Ahmed, A. A., Pihlap, E., Reinhard,
1206 C. T., and Planavsky, N. J.: Mitigation of soil nitrous oxide emissions during maize
1207 production with basalt amendments, Front. Clim., 5, 1203043,
1208 https://doi.org/10.3389/fclim.2023.1203043, 2023.

1209 Crilley, L. R., Kramer, L. J., Ouyang, B., Duan, J., Zhang, W., Tong, S., Ge, M., Tang, K., Qin,
1210 M., Xie, P., Shaw, M. D., Lewis, A. C., Mehra, A., Bannan, T. J., Worrall, S. D., Priestley,
1211 M., Bacak, A., Coe, H., Allan, J., and Bloss, W. J.: Intercomparison of nitrous acid
1212 (HONO) measurement techniques in a megacity (Beijing), Atmos. Meas. Tech. Discuss.
1213 [preprint], https://doi.org/10.5194/amt-2019-139, 2019.

1214 Crilley, L. R., Lao, M., Salehpoor, L., and VandenBoer, T. C.: Emerging investigator series: an
1215 instrument to measure and speciate the total reactive nitrogen budget indoors: description
1216 and field measurements, Environ. Sci. Process. Impacts, 25, 389–404,
1217 https://doi.org/10.1039/d2em00446a, 2023.

1218 Degaspari, I. A. M., Soares, J. R., Montezano, Z. F., Del Grosso, S. J., Vitti, A. C., Rossetto, R.,
1219 and Cantarella, H.: Nitrogen sources and application rates affect emissions of N2O and
1220 NH3 in sugarcane, Nutr. Cycl. Agroecosyst., 116, 329–344,
1221 https://doi.org/10.1007/s10705-019-10045-w, 2020.

1222 Delaria, E. R. and Cohen, R. C.: Measurements of Atmosphere-Biosphere Exchange of Oxidized
1223 Nitrogen and Implications for the Chemistry of Atmospheric NOx, Acc. Chem. Res., 56,
1224 1720–1730, https://doi.org/10.1021/acs.accounts.3c00090, 2023.

1225 Dennis, R. L., Mathur, R., Pleim, J. E., and Walker, J. T.: Fate of ammonia emissions at the local
1226 to regional scale as simulated by the Community Multiscale Air Quality model, Atmos.
1227 Pollut. Res., 1, 207–214, https://doi.org/10.5094/APR.2010.027, 2010.

1228 Ebnesajjad, S.: Introduction to Fluoropolymers, in: Applied Plastics Engineering Handbook:
1229 Processing, Materials, and Applications, 2nd edn., Elsevier, 55–71,
1230 https://doi.org/10.1016/B978-0-323-39040-8.00003-1, 2017.

1231 Edwards, T. M., Puglis, H. J., Kent, D. B., Durán, J. L., Bradshaw, L. M., and Farag, A. M.:
1232 Ammonia and aquatic ecosystems – A review of global sources, biogeochemical cycling,
1233 and effects on fish, Sci. Total Environ., 907, 167911,
1234 https://doi.org/10.1016/j.scitotenv.2023.167911, 2024.

Ellis, R. A., Murphy, J. G., Pattey, E., Van Haarlem, R., O'Brien, J. M., and Herndon, S. C.: Characterizing a Quantum Cascade Tunable Infrared Laser Differential Absorption Spectrometer (QC-TILDAS) for measurements of atmospheric ammonia, Atmos. Meas. Tech., 3, 397–406, https://doi.org/10.5194/amt-3-397-2010, 2010.

Finlayson-Pitts, B. J., Wingen, L. M., Sumner, A. L., Syomin, D., and Ramazan, K. A.: The heterogeneous hydrolysis of NO2 in laboratory systems and in outdoor and indoor atmospheres: An integrated mechanism, Phys. Chem. Chem. Phys., 5, 223–242, https://doi.org/10.1039/b208564j, 2003.

Fowler, D., Coyle, M., Skiba, U., Sutton, M. A., Cape, J. N., Reis, S., Sheppard, L. J., Jenkins, A., Grizzetti, B., Galloway, J. N., Vitousek, P., Leach, A., Bouwman, A. F., Butterbach-Bahl, K., Dentener, F., Stevenson, D., Amann, M., and Voss, M.: The global nitrogen cycle in the twenty-first century, Philos. Trans. R. Soc. B Biol. Sci., 368, 20130164, https://doi.org/10.1098/rstb.2013.0164, 2013.

Geddes, J. A. and Murphy, J. G.: Observations of reactive nitrogen oxide fluxes by eddy covariance above two midlatitude North American mixed hardwood forests, Atmos. Chem. Phys., 14, 2939–2957, https://doi.org/10.5194/acp-14-2939-2014, 2014.

George, C., Ammann, M., D'Anna, B., Donaldson, D. J., and Nizkorodov, S. A.: Heterogeneous Photochemistry in the Atmosphere, Chem. Rev., 115, 4218–4258, https://doi.org/10.1021/cr500648z, 2015.

Gong, C., Wang, Y., Tian, H., Kou-Giesbrecht, S., Vuichard, N., and Zaehle, S.: Uncertainties in fertilizer-induced emissions of soil nitrogen oxide and the associated impacts on ground-level ozone and methane, EGUsphere [preprint], https://doi.org/10.5194/egusphere-2025-1416, 2025.

Govoni Brondi, M., Bortoletto-Santos, R., Farias, J. G., Farinas, C. S., Ammar, M., Ribeiro, C., Williams, C., and Baltrusaitis, J.: Mechanochemically Synthesized Nitrogen-Efficient Mg- and Zn-Ammonium Carbonate Fertilizers, ACS Sustain. Chem. Eng., 12, 6182–6193, https://doi.org/10.1021/acssuschemeng.3c07785, 2024.

Ha, P. T. M., Kanaya, Y., Taketani, F., Andres Hernandez, M. D., Schreiner, B., Pfeilsticker, K., and Sudo, K.: Implementation of HONO into the chemistry-climate model CHASER (V4.0): Roles in tropospheric chemistry, Geosci. Model Dev., 16, 927–960, https://doi.org/10.5194/gmd-16-927-2023, 2023.

He, Y., Zhou, X., Hou, J., Gao, H., and Bertman, S. B.: Importance of dew in controlling the air-surface exchange of HONO in rural forested environments, Geophys. Res. Lett., 33, L02813, https://doi.org/10.1029/2005GL024348, 2006.

Huang, G., Zhou, X., Deng, G., Qiao, H., and Civerolo, K.: Measurements of atmospheric nitrous acid and nitric acid, Atmos. Environ., 36, 2225–2235, https://doi.org/10.1016/S1352-2310(02)00170-X, 2002.

Huber, D. E., Kort, E. A., and Steiner, A. L.: Soil Moisture, Soil NOx and Regional Air Quality in the Agricultural Central United States, J. Geophys. Res. Atmos., 129, e2024JD041015, https://doi.org/10.1029/2024JD041015, 2024.

IPCC: Climate Change 2021 – The Physical Science Basis, Cambridge University Press, Cambridge, https://doi.org/10.1017/9781009157896, 2023.

Jang, J.-H., Hong, J., Kim, J. B., Park, S., Hwang, K., Kim, J., Kim, J. Y., Bae, G.-N., Kim, S., and Kim, K. H.: Influence of atmospheric ammonia on secondary inorganic aerosol formation in PM2.5 during spring 2024 in the Hongseong area, Republic of Korea, Atmos. Environ., 321, 121363, https://doi.org/10.1016/j.atmosenv.2025.121363, 2025.

Kamboures, M. A., Raff, J. D., Miller, Y., Phillips, L. F., Finlayson-Pitts, B. J., and Gerber, R. B.: Complexes of HNO3 and NO3− with NO2 and N2O4, and their potential role in atmospheric HONO formation, Phys. Chem. Chem. Phys., 10, 6019–6032, https://doi.org/10.1039/b805330h, 2008.

Kamp, J. N., Häni, C., Nyord, T., Feilberg, A., and Sørensen, L. L.: The aerodynamic gradient method: Implications of non-simultaneous measurements at alternating heights, Atmosphere, 11, 1067, https://doi.org/10.3390/atmos11101067, 2020.

Kleffmann, J., Gavriloaiei, T., Hofzumahaus, A., Holland, F., Koppmann, R., Rupp, L., Schlosser, E., Siese, M., and Wahner, A.: Daytime formation of nitrous acid: A major source of OH radicals in a forest, Geophys. Res. Lett., 32, L05818, https://doi.org/10.1029/2005GL022524, 2005.

Kolari, P., Bäck, J., Taipale, R., Ruuskanen, T. M., Kajos, M. K., Rinne, J., Kulmala, M., and Hari, P.: Evaluation of accuracy in measurements of VOC emissions with dynamic chamber system, Atmos. Environ., 62, 344–351, https://doi.org/10.1016/j.atmosenv.2012.08.054, 2012.

Kool, D. M., Wrage, N., Zechmeister-Boltenstern, S., Pfeffer, M., Brus, D., Oenema, O., and Van Groenigen, J. W.: Nitrifier denitrification can be a source of N2O from soil: A revised approach to the dual-isotope labelling method, Eur. J. Soil Sci., 61, 759–772, https://doi.org/10.1111/j.1365-2389.2010.01270.x, 2010.

Lao, M., Crilley, L. R., Salehpoor, L., Furlani, T. C., Bourgeois, I., Neuman, J. A., Rollins, A. W., Veres, P. R., Washenfelder, R. A., Womack, C. C., Young, C. J., and VandenBoer, T. C.: A portable, robust, stable, and tunable calibration source for gas-phase nitrous acid (HONO), Atmos. Meas. Tech., 13, 5873–5890, https://doi.org/10.5194/amt-13-5873-2020, 2020.

Laufs, S., Cazaunau, M., Stella, P., Kurtenbach, R., Cellier, P., Mellouki, A., Loubet, B., and Kleffmann, J.: Diurnal fluxes of HONO above a crop rotation, Atmos. Chem. Phys., 17, 6907–6923, https://doi.org/10.5194/acp-17-6907-2017, 2017.

Lee, B. H., Lopez-Hilfiker, F. D., Mohr, C., Kurtén, T., Worsnop, D. R., and Thornton, J. A.: An iodide-adduct high-resolution time-of-flight chemical-ionization mass spectrometer:

Application to atmospheric inorganic and organic compounds, Environ. Sci. Technol., 48, 6309–6317, https://doi.org/10.1021/es500362a, 2014.

Lehnert, N., Musselman, B. W., Seefeldt, L. C., and Gutenberg-university, J.: Grand Challenges in the nitrogen cycle, Chem. Soc. Rev., 50, 3640–3646, https://doi.org/10.1039/d0cs00923g, 2021.

Li, L., Fan, W., Kang, X., Wang, Y., Cui, X., Xu, C., Griffin, K. L., and Hao, Y.: Responses of greenhouse gas fluxes to climate extremes in a semiarid grassland, Atmos. Environ., 142, 32–42, https://doi.org/10.1016/j.atmosenv.2016.07.039, 2016.

Lide, D. R.: CRC Handbook of Chemistry and Physics, 90th edn., CRC Press/Taylor & Francis, Boca Raton, FL, 2009.

Lipiec, J., Walczak, R., Witkowska-Walczak, B., Nosalewicz, A., Słowińska-Jurkiewicz, A., and Sławiński, C.: The effect of aggregate size on water retention and pore structure of two silt loam soils of different genesis, Soil Tillage Res., 97, 239–246, https://doi.org/10.1016/j.still.2007.10.001, 2007.

Liu, L., Zhang, X., Xu, W., Liu, X., Li, Y., Wei, J., Wang, Z., and Lu, X.: Ammonia volatilization as the major nitrogen loss pathway in dryland agro-ecosystems, Environ. Pollut., 265, 114862, https://doi.org/10.1016/j.envpol.2020.114862, 2020.

Liu, Z., Zheng, X., Li, Y., Yu, J., Ding, H., Sveen, T. R., and Zhang, Y.: Soil moisture determines nitrous oxide emission and uptake, Sci. Total Environ., 822, 153566, https://doi.org/10.1016/j.scitotenv.2022.153566, 2022.

Ludwig, J., Meixner, F. X., Vogel, B., and Forstner, J.: Soil-air exchange of nitric oxide: An overview of processes, environmental factors, and modeling studies, Biogeochemistry, 52, 225–257, https://doi.org/10.1023/A:1006424330555, 2001.

Luo, X., Zhang, M., Ni, Y., and Shen, G.: Mitigation strategies for NH3 and N2O emissions in greenhouse agriculture: Insights into fertilizer management and nitrogen emission mechanisms, Environ. Technol. Innov., 37, 103995, https://doi.org/10.1016/j.eti.2024.103995, 2025.

Maggiotto, S. R., Webb, J. A., and Thurtell, G. W.: Nitrous and Nitrogen Oxide Emissions from Turfgrass Receiving Different Forms of Nitrogen Fertilizer, J. Environ. Qual., 29, 621–630, https://doi.org/10.2134/jeq2000.00472425002900020033x, 2000.

Manco, A., Giaccone, M., Vitale, L., Maglione, G., Riccardi, M., Di Matteo, B., Esposito, A., Magliulo, V., and Tedeschi, A.: Comparative Effects of Nitrogen Fertigation and Granular Fertilizer Application on Pepper Yield and Soil GHGs Emissions, Horticulturae, 11, 708, https://doi.org/10.3390/horticulturae11060708, 2025.

Mangalassery, S., Sjögersten, S., Sparkes, D. L., Sturrock, C. J., and Mooney, S. J.: The effect of soil aggregate size on pore structure and its consequence on emission of greenhouse gases, Soil Tillage Res., 132, 39–46, https://doi.org/10.1016/j.still.2013.05.003, 2013.

Meusel, H., Tamm, A., Kuhn, U., Wu, D., Leifke, A. L., Fiedler, S., Ruckteschler, N., Yordanova, P., Lang-Yona, N., Pöhlker, M., Lelieveld, J., Hoffmann, T., Pöschl, U., Su, H., Weber, B., and Cheng, Y.: Emission of nitrous acid from soil and biological soil crusts represents an important source of HONO in the remote atmosphere in Cyprus, Atmos. Chem. Phys., 18, 799–813, https://doi.org/10.5194/acp-18-799-2018, 2018.

Milford, C., Theobald, M. R., Nemitz, E., Hargreaves, K. J., Horvath, L., Raso, J., Dämmgen, U., Neftel, A., Jones, S. K., Hensen, A., Loubet, B., Cellier, P., and Sutton, M. A.: Ammonia fluxes in relation to cutting and fertilization of an intensively managed grassland derived from an inter-comparison of gradient measurements, Biogeosciences, 6, 819–834, https://doi.org/10.5194/bg-6-819-2009, 2009.

Min, K. E., Pusede, S. E., Browne, E. C., LaFranchi, B. W., and Cohen, R. C.: Eddy covariance fluxes and vertical concentration gradient measurements of NO and NO2 over a ponderosa pine ecosystem: Observational evidence for within-canopy chemical removal of NOx, Atmos. Chem. Phys., 14, 5495–5512, https://doi.org/10.5194/acp-14-5495-2014, 2014.

Mochizuki, T., Amagai, T., and Tani, A.: Effects of soil water content and elevated CO2 concentration on the monoterpene emission rate of Cryptomeria japonica, Sci. Total Environ., 634, 900–908, https://doi.org/10.1016/j.scitotenv.2018.04.025, 2018.

Moravek, A., Foken, T., and Trebs, I.: Application of a GC-ECD for measurements of biosphere-atmosphere exchange fluxes of peroxyacetyl nitrate using the relaxed eddy accumulation and gradient method, Atmos. Meas. Tech., 7, 2097–2119, https://doi.org/10.5194/amt-7-2097-2014, 2014.

Moravek, A., Singh, S., Pattey, E., Pelletier, L., and Murphy, J. G.: Measurements and quality control of ammonia eddy covariance fluxes: A new strategy for high-frequency attenuation correction, Atmos. Meas. Tech., 12, 6059–6078, https://doi.org/10.5194/amt-12-6059-2019, 2019.

Mosier, A. R.: Exchange of Gaseous Nitrogen Compounds Between Terrestrial Systems and the Atmosphere, in: Nitrogen in the Environment, 2nd edn., Elsevier, 443–462, https://doi.org/10.1016/B978-0-12-374347-3.00013-5, 2008.

Mushinski, R. M., Phillips, R. P., Payne, Z. C., Abney, R. B., Jo, I., Fei, S., Pusede, S. E., White, J. R., Rusch, D. B., and Raff, J. D.: Microbial mechanisms and ecosystem flux estimation for aerobic NOy emissions from deciduous forest soils, P. Natl. Acad. Sci. USA, 116, 2138–2145, https://doi.org/10.1073/pnas.1814632116, 2019.

Neuman, J. A., Trainer, M., Brown, S. S., Min, K. E., Nowak, J. B., Parrish, D. D., Peischl, J., Pollack, I. B., Roberts, J. M., Ryerson, T. B., and Veres, P. R.: HONO emission and production determined from airborne measurements over the Southeast U.S., J. Geophys. Res. Atmos., 121, 9237–9250, https://doi.org/10.1002/2016JD025197, 2016.

Nodeh-Farahani, D., Bentley, J. N., Crilley, L. R., Caputo, C. B., and VandenBoer, T. C.: A boron dipyrromethene (BODIPY) based probe for selective passive sampling of atmospheric

nitrous acid (HONO) indoors, Analyst, 146, 5756–5766, https://doi.org/10.1039/d1an01089a, 2021.

Okiti, I., Efakwu, G., Pindus, M., and Kasak, K.: Environmental and biogeochemical drivers of CH4 and N2O flux variability in treatment wetlands, Ecol. Eng., 219, 107705, https://doi.org/10.1016/j.ecoleng.2025.107705, 2025.

Oswald, R., Behrendt, T., Ermel, M., Wu, D., Su, H., Cheng, Y., Breuninger, C., Moravek, A., Mougin, E., Delon, C., Loubet, B., Pommerening-Röser, A., Sörgel, M., Pöschl, U., Hoffmann, T., Andreae, M. O., Meixner, F. X., and Trebs, I.: HONO emissions from soil bacteria as a major source of atmospheric reactive nitrogen, Science, 341, 1233–1235, https://doi.org/10.1126/science.1242266, 2013.

Pan, B., Lam, S. K., Mosier, A., Luo, Y., and Chen, D.: Ammonia volatilization from synthetic fertilizers and its mitigation strategies: A global synthesis, Agric. Ecosyst. Environ., 232, 283–289, https://doi.org/10.1016/j.agee.2016.08.019, 2016.

Pan, B., Xia, L., Lam, S. K., Wang, E., Zhang, Y., Mosier, A., and Chen, D.: A global synthesis of soil denitrification: Driving factors and mitigation strategies, Agric. Ecosyst. Environ., 327, 107850, https://doi.org/10.1016/j.agee.2021.107850, 2022.

Pape, L., Ammann, C., Nyfeler-Brunner, A., Spirig, C., Hens, K., and Meixner, F. X.: An automated dynamic chamber system for surface exchange measurement of non-reactive and reactive trace gases of grassland ecosystems, Biogeosciences, 6, 405–429, https://doi.org/10.5194/bg-6-405-2009, 2009.

Paulot, F., Jacob, D. J., Pinder, R. W., Bash, J. O., Travis, K., and Henze, D. K.: Ammonia emissions in the United States, European Union, and China derived by high-resolution inversion of ammonium wet deposition data: Interpretation with a new agricultural emissions inventory (MASAGE_NH3), J. Geophys. Res. Atmos., 119, 4343–4364, https://doi.org/10.1002/2013JD021130, 2014.

Plake, D., Sörgel, M., Stella, P., Held, A., and Trebs, I.: Influence of meteorology and anthropogenic pollution on chemical flux divergence of the NO-NO2-O3 triad above and within a natural grassland canopy, Biogeosciences, 12, 945–959, https://doi.org/10.5194/bg-12-945-2015, 2015a.

Plake, D., Stella, P., Moravek, A., Mayer, J. C., Ammann, C., Held, A., and Trebs, I.: Comparison of ozone deposition measured with the dynamic chamber and the eddy covariance method, Agric. For. Meteorol., 206, 97–112, https://doi.org/10.1016/j.agrformet.2015.02.014, 2015b.

Possanzini, M., Febo, A., and Liberti, A.: New design of a high-performance denuder for the sampling of atmospheric pollutants, Atmos. Environ., 17, 2605–2610, https://doi.org/10.1016/0004-6981(83)90089-6, 1983.

Pugliese, G., Ingrisch, J., Meredith, L. K., Pfannerstill, E. Y., Klüpfel, T., Meeran, K., Byron, J., Purser, G., Gil-Loaiza, J., van Haren, J., Dontsova, K., Kreuzwieser, J., Ladd, S. N., Werner, C., and Williams, J.: Effects of drought and recovery on soil volatile organic

compound fluxes in an experimental forest, Nat. Commun., 14, 5064, https://doi.org/10.1038/s41467-023-40661-8, 2023.

Purchase, M. L., Bending, G. D., and Mushinski, R. M.: Spatiotemporal Variations of Soil Reactive Nitrogen Oxide Fluxes across the Anthropogenic Landscape, Environ. Sci. Technol., 57, 16348–16360, https://doi.org/10.1021/acs.est.3c05849, 2023.

Ramazan, K. A., Syomin, D., and Finlayson-Pitts, B. J.: The photochemical production of HONO during the heterogeneous hydrolysis of NO2, Phys. Chem. Chem. Phys., 6, 3836–3843, https://doi.org/10.1039/b402195a, 2004.

Reed, C., Brumby, C. A., Crilley, L. R., Kramer, L. J., Bloss, W. J., Seakins, P. W., Lee, J. D., and Carpenter, L. J.: HONO measurement by differential photolysis, Atmos. Meas. Tech., 9, 2483–2495, https://doi.org/10.5194/amt-9-2483-2016, 2016.

Ren, X., Sanders, J. E., Rajendran, A., Weber, R. J., Goldstein, A. H., Pusede, S. E., Browne, E. C., Min, K. E., and Cohen, R. C.: A relaxed eddy accumulation system for measuring vertical fluxes of nitrous acid, Atmos. Meas. Tech., 4, 2093–2103, https://doi.org/10.5194/amt-4-2093-2011, 2011.

Ren, Y., Stieger, B., Spindler, G., Grosselin, B., Mellouki, A., Tuch, T., Wiedensohler, A., and Herrmann, H.: Role of the dew water on the ground surface in HONO distribution: A case measurement in Melpitz, Atmos. Chem. Phys., 20, 13069–13089, https://doi.org/10.5194/acp-20-13069-2020, 2020.

Richardson, K., Steffen, W., Lucht, W., Bendtsen, J., Cornell, S. E., Donges, J. F., Drüke, M., Fetzer, I., Bala, G., Von Bloh, W., Feulner, G., Fiedler, S., Gerten, D., Gleeson, T., Hofmann, M., Huiskamp, W., Kummu, M., Mohan, C., Nogués-Bravo, D., and Rockström, J.: Earth beyond six of nine planetary boundaries, Sci. Adv., 9, eadh2458, https://doi.org/10.1126/sciadv.adh2458, 2023.

Scharko, N. K., Schütte, U. M. E., Berke, A. E., Banina, L., Peel, H. R., Donaldson, M. A., Hemmerich, C., White, J. R., and Raff, J. D.: Combined Flux Chamber and Genomics Approach Links Nitrous Acid Emissions to Ammonia Oxidizing Bacteria and Archaea in Urban and Agricultural Soil, Environ. Sci. Technol., 49, 13825–13834, https://doi.org/10.1021/acs.est.5b00838, 2015.

Schindlbacher, A., Zechmeister-Boltenstern, S., and Jandl, R.: Carbon losses due to soil warming: Do autotrophic and heterotrophic soil respiration respond equally?, Glob. Change Biol., 15, 901–913, https://doi.org/10.1111/j.1365-2486.2008.01757.x, 2009.

Schlesinger, W. H.: Biogeochemistry: An Analysis of Global Change, 4th edn., Academic Press, https://doi.org/10.1016/C2018-0-03255-3, 2020.

Seinfeld, J. H. and Pandis, S. N.: Atmospheric Chemistry and Physics: From Air Pollution to Climate Change, 2nd edn., John Wiley & Sons, Hoboken, 2006.

Shah, S. B., Grabow, G. L., and Westerman, P. W.: Ammonia adsorption in five types of flexible tubing materials, Appl. Eng. Agric., 22, 919–923, https://doi.org/10.13031/2013.22253, 2006.

Song, Y., Xue, C., Zhang, Y., Liu, P., Bao, F., Li, X., and Mu, Y.: Measurement report: exchange fluxes of HONO over agricultural fields in the North China Plain, Atmos. Chem. Phys., https://doi.org/10.5281/zenodo.8115973, 2023.

Sörgel, M., Trebs, I., Wu, D., and Held, A.: A comparison of measured HONO uptake and release with calculated source strengths in a heterogeneous forest environment, Atmos. Chem. Phys., 15, 9237–9251, https://doi.org/10.5194/acp-15-9237-2015, 2015.

Spataro, F. and Ianniello, A.: Sources of atmospheric nitrous acid: State of the science, current research needs, and future prospects, J. Air Waste Manage. Assoc., 64, 1232–1250, https://doi.org/10.1080/10962247.2014.952846, 2014.

Stepniewski, W., Stepniewska, Z., and Rozej, A.: Gas Exchange in Soils, in: Soil Management: Building a Stable Base for Agriculture, American Society of Agronomy and Soil Science Society of America, Madison, 117–144, https://doi.org/10.2136/2011.soilmanagement.c8, 2015.

Su, H., Cheng, Y., Oswald, R., Behrendt, T., Trebs, I., Meixner, F. X., Andreae, M. O., Cheng, P., Zhang, Y., and Pöschl, U.: Soil nitrite as a source of atmospheric HONO and OH radicals, Science, 333, 1616–1618, https://doi.org/10.1126/science.1207687, 2011.

Tang, K., Qin, M., Duan, J., Fang, W., Meng, F., Liang, S., Xie, P., Liu, J., Liu, W., Xue, C., and Mu, Y.: A dual dynamic chamber system based on IBBCEAS for measuring fluxes of nitrous acid in agricultural fields in the North China Plain, Atmos. Environ., 196, 10–19, https://doi.org/10.1016/j.atmosenv.2018.09.059, 2019.

Tang, K., Qin, M., Fang, W., Duan, J., Meng, F., Ye, K., Zhang, H., Xie, P., Liu, J., Liu, W., Feng, Y., Huang, Y., and Ni, T.: An automated dynamic chamber system for exchange flux measurement of reactive nitrogen oxides (HONO and NOX) in farmland ecosystems of the Huaihe River Basin, China, Sci. Total Environ., 745, 140867, https://doi.org/10.1016/j.scitotenv.2020.140867, 2020.

Taylor, N. M., Wagner-Riddle, C., Thurtell, G. W., & Beauchamp, E. G. Nitric oxide fluxes from an agricultural soil using a flux-gradient method, J. Geophys. Res. Atmos., 104, 12213–12220, https://doi.org/10.1029/1999JD900181, 1999.

Tian, H., Pan, N., Thompson, R. L., Canadell, J. G., Suntharalingam, P., Regnier, P., Davidson, E. A., Prather, M., Ciais, P., Muntean, M., Pan, S., Winiwarter, W., Zaehle, S., Zhou, F., Jackson, R. B., Bange, H. W., Berthet, S., Bian, Z., Bianchi, D., and Zhu, Q.: Global nitrous oxide budget (1980–2020), Earth Syst. Sci. Data, 16, 2543–2604, https://doi.org/10.5194/essd-16-2543-2024, 2024.

Vaittinen, O., Metsälä, M., Persijn, S., Vainio, M., and Halonen, L.: Adsorption of ammonia on treated stainless steel and polymer surfaces, Appl. Phys. B, 115, 185–196, https://doi.org/10.1007/s00340-013-5590-3, 2014.

VandenBoer, T. C., Brown, S. S., Murphy, J. G., Keene, W. C., Young, C. J., Pszenny, A. A. P., Kim, S., Warneke, C., De Gouw, J. A., Maben, J. R., Wagner, N. L., Riedel, T. P., Thornton, J. A., Wolfe, D. E., Dubé, W. P., Öztürk, F., Brock, C. A., Grossberg, N., Lefer, B., and Roberts, J. M.: Understanding the role of the ground surface in HONO vertical structure: High resolution vertical profiles during NACHTT-11, J. Geophys. Res. Atmos., 118, 10155–10171, https://doi.org/10.1002/jgrd.50721, 2013.

VandenBoer, T. C., Young, C. J., Talukdar, R. K., Markovic, M. Z., Brown, S. S., Roberts, J. M., and Murphy, J. G.: Nocturnal loss and daytime source of nitrous acid through reactive uptake and displacement, Nat. Geosci., 8, 55–60, https://doi.org/10.1038/ngeo2298, 2015.

Von Der Heyden, L., Wißdorf, W., Kurtenbach, R., and Kleffmann, J.: A relaxed eddy accumulation (REA) LOPAP system for flux measurements of nitrous acid (HONO), Atmos. Meas. Tech., 15, 1983–2000, https://doi.org/10.5194/amt-15-1983-2022, 2022.

Wang, T., Fu, X., Wu, D., Wang, M., Lu, K., Mu, Y., Liu, Z., Zhang, Y., and Wang, T.: Agricultural Fertilization Aggravates Air Pollution by Stimulating Soil Nitrous Acid Emissions at High Soil Moisture, Environ. Sci. Technol., 55, 14556–14566, https://doi.org/10.1021/acs.est.1c04134, 2021.

Wang, Y., Fu, X., Wang, T., Ma, J., Gao, H., Wang, X., and Pu, W.: Large Contribution of Nitrous Acid to Soil-Emitted Reactive Oxidized Nitrogen and Its Effect on Air Quality, Environ. Sci. Technol., 56, 15280–15290, https://doi.org/10.1021/acs.est.2c07793, 2022.

Whitehead, J. D., Twigg, M., Famulari, D., Nemitz, E., Sutton, M. A., Gallagher, M. W., and Fowler, D.: Evaluation of laser absorption spectroscopic techniques for eddy covariance flux measurements of ammonia, Environ. Sci. Technol., 42, 2041–2046, https://doi.org/10.1021/es702616f, 2008.

Wolff, V., Trebs, I., Ammann, C., and Meixner, F. X.: Aerodynamic gradient measurements of the NH3-HNO3-NH4NO3 triad using a wet chemical instrument: an analysis of precision requirements and flux errors, Atmos. Meas. Tech., 3, 187–208, https://doi.org/10.5194/amt-3-187-2010, 2010.

Wu, D., Deng, L., Liu, Y., Xi, D., Zou, H., Sha, Z., Pan, Y., Hou, L., and Liu, M.: Comparisons of the effects of different drying methods on soil nitrogen fractions: Insights into emissions of reactive nitrogen gases (HONO and NO), Acta Ecol. Sin., 40, 1–10, https://doi.org/10.1080/16742834.2020.1733388, 2020.

Wu, D., Horn, M. A., Behrendt, T., Müller, S., Li, J., Cole, J. A., Xie, B., Ju, X., Li, G., Ermel, M., Oswald, R., Fröhlich-Nowoisky, J., Hoor, P., Hu, C., Liu, M., Andreae, M. O., Pöschl, U., Cheng, Y., Su, H., and Sörgel, M.: Soil HONO emissions at high moisture content are driven by microbial nitrate reduction to nitrite: tackling the HONO puzzle, ISME J., 13, 1688–1699, https://doi.org/10.1038/s41396-019-0379-y, 2019.

Wu, D., Zhang, J., Wang, M., An, J., Wang, R., Haider, H., Xu-Ri, Huang, Y., Zhang, Q., Zhou, F., Tian, H., Zhang, X., Deng, L., Pan, Y., Chen, X., Yu, Y., Hu, C., Wang, R., Song, Y., and Liu, M.: Global and Regional Patterns of Soil Nitrous Acid Emissions and Their

Acceleration of Rural Photochemical Reactions, J. Geophys. Res. Atmos., 127, e2021JD036379, https://doi.org/10.1029/2021JD036379, 2022.

Xue, C., Ye, C., Lu, K., Liu, P., Zhang, C., Su, H., Bao, F., Cheng, Y., Wang, W., Liu, Y., Catoire, V., Ma, Z., Zhao, X., Song, Y., Ma, X., McGillen, M. R., Mellouki, A., Mu, Y., and Zhang, Y.: Reducing soil-emitted nitrous acid as a feasible strategy for tackling ozone pollution, Environ. Sci. Technol., 58, 9227–9235, https://doi.org/10.1021/acs.est.4c01070, 2024.

Yang, J. Y., Drury, C. F., Jiang, R., Worth, D. E., Bittman, S., Grant, B. B., and Smith, W. N.: Reactive nitrogen losses from Canadian agricultural soils over 36 years, Ecol. Model., 495, 110809, https://doi.org/10.1016/j.ecolmodel.2024.110809, 2024.

Young, C. J., Washenfelder, R. A., Roberts, J. M., Mielke, L. H., Osthoff, H. D., Tsai, C., Pikelnaya, O., Stutz, J., Veres, P. R., Cochran, A. K., VandenBoer, T. C., Flynn, J., Grossberg, N., Haman, C. L., Lefer, B., Stark, H., Graus, M., de Gouw, J., Gilman, J. B., and Brown, S. S.: Vertically Resolved Measurements of Nighttime Radical Reservoirs in Los Angeles and Their Contribution to the Urban Radical Budget, Environ. Sci. Technol., 46, 10965–10973, https://doi.org/10.1021/es302206a, 2012.

Zhang, S., Sarwar, G., Xing, J., Chu, B., Xue, C., Sarav, A., Ding, D., Zheng, H., Mu, Y., Duan, F., Ma, T., and He, H.: Improving the representation of HONO chemistry in CMAQ and examining its impact on haze over China, Atmos. Chem. Phys., 21, 15809–15826, https://doi.org/10.5194/acp-21-15809-2021, 2021.

Zhou, S., Young, C. J., VandenBoer, T. C., Kowal, S. F., and Kahan, T. F.: Time-Resolved Measurements of Nitric Oxide, Nitrogen Dioxide, and Nitrous Acid in an Occupied New York Home, Environ. Sci. Technol., 52, 8355–8364, https://doi.org/10.1021/acs.est.8b01792, 2018.

Zörner, J., Penning De Vries, M., Beirle, S., Sihler, H., Veres, P. R., Williams, J., and Wagner, T.: Multi-satellite sensor study on precipitation-induced emission pulses of NOx from soils in semi-arid ecosystems, Atmos. Chem. Phys., 16, 9457–9487, https://doi.org/10.5194/acp-16-9457-2016, 2016.